Article

Discovery of INCB159020, an Orally Bioavailable KRAS G12D Inhibitor

Qinda Ye, Artem Shvartsbart, Zhenwu Li, Pei Gan, Rocco L. Policarpo, Chao Qi, Jeremy J. Roach, Wenyu Zhu, Matthew S. McCammant, Bin Hu, Gencheng Li, Haolin Yin, Peter Carlsen, Gia Hoang, Le Zhao, Robert Susick, Fenglei Zhang, Cheng-Tsung Lai, Abdellah Allali Hassani, Leslie B. Epling, Alexandra Gallion, Kerri Kurzeja-Lipinski, Karen Gallagher, Valerie Roman, Matthew R. Farren, Weixi Kong, Marc C. Deller, Guofeng Zhang, Maryanne Covington, Sharon Diamond, Sunkyu Kim, Wenqing Yao, Alexander Sokolsky,* and Xiaozhao Wang

Read Online

ACCESS | Metrics & More | Article Recommendations | Supporting Information

KRAS Exchange: >8 μM

KRAS SPR: <1 pM
pERK WB: 451 nM
No oral exposure

INCB159020
KRAS SPR: 2.2 nM
pERK WB: 331 nM
Oral exposure in non-human primate
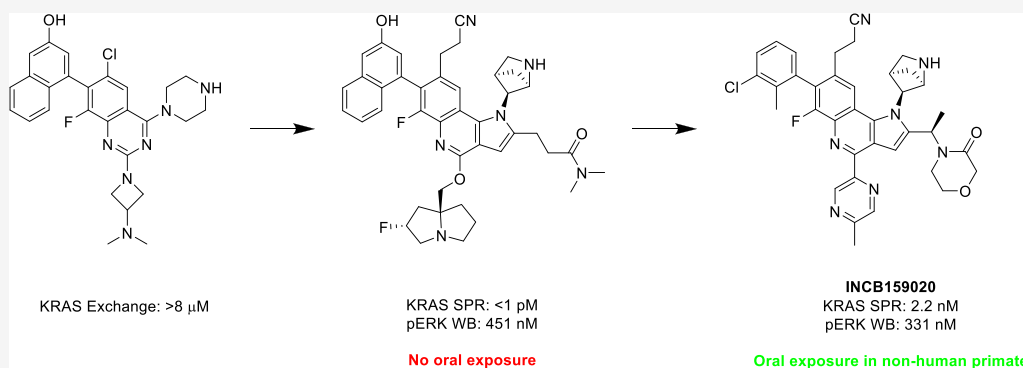
ABSTRACT: The inhibition of mutant KRAS proteins has emerged as a promising approach for treating KRAS-driven cancers, as evidenced by the clinical success of KRAS G12C inhibitors. KRAS G12D, the most common mutant, promises significant expansion of the addressable patient population; however, the reduced nucleophilicity of aspartate compared to cysteine poses significant challenges in balancing sufficient potency with ADME properties to support oral exposure. Herein, we describe the discovery of KRAS G12D inhibitor **23** (**INCB159020**), which achieves oral exposure in nonhuman primate (NHP). Starting from a weakly potent hit, structure-based drug design was utilized to drive significant potency. Focus on molecular rigidity and balanced polarity then allowed for successful optimization of properties required for oral exposure.

INTRODUCTION

Kirsten rat sarcoma virus (KRAS) is a GTPase that acts as a master regulator of the RAS/MAPK and PI3K/AKT pathways governing cell growth, differentiation, proliferation and survival.[1] Upon binding GTP, KRAS enters an activated state, signaling through Raf and PI3K to stimulate the production of growth factors. As GTP is hydrolyzed to GDP, KRAS enters a GDP-bound off state. Active/inactive state cycling is achieved through the action of Guanine Nucleotide Exchange Factors (GEFs) such as SOS1.[2] As a consequence of its central status, KRAS is frequently misregulated in a variety of human cancers, including nonsmall cell lung (NSCLC), pancreatic and colorectal cancer. In fact, it is estimated that 20% of human tumors are driven by KRAS mutations.[3,4] Mutations can occur at a number of positions, but are most frequently localized to Gly12, Gly13 and Gln61. These mutations decrease the intrinsic hydrolysis rate of GTP, leading to buildup of the activated form,

constitutive pathway activation and uncontrolled cellular proliferation. When mutated, KRAS has been shown to act as a key driver of proliferation. This fact, combined with the high prevalence of KRAS mutations across the deadliest of human cancers, makes KRAS a critical target for drug discovery.

However, KRAS has proven to present a formidable challenge to discovery efforts, due to the exceptional binding affinity to GTP preventing direct inhibition of the active site. A significant breakthrough was made in 2013, when Shokat and coworkers described the discovery of a new pocket adjacent to the

nucleoside binding region, which could be accessed by covalently modifying the cysteine residue present in the KRAS G12C mutant.[5] Further optimization by a number of groups led to the identification of numerous potent and efficacious clinical KRAS G12C inhibitors,[6−11] culminating with the FDA approval of sotorasib and adagrasib for the treatment of KRAS G12C-mutated NSCLC in 2021 and 2022 respectively.

The success of KRAS G12C inhibitors led to increased interest in inhibiting other mutant forms of KRAS. Among these, the G12D mutation is the most prevalent mutation observed in KRAS and represents a significant additional patient populations, in particular in pancreatic (37% of tumors) and colorectal (12% of tumors) indications. However, the KRAS G12D mutant presents a unique challenge, owing to the attenuated nucleophilicity of the aspartic acid, rendering a covalent approach uncertain. While covalent interactions with aspartic acid are possible,[12−14] the requirement of increased electrophilicity raises concerns with respect to selectivity and safety. An alternative approach involves the removal of the warhead in pursuit of a reversible inhibitor. Researchers at Mirati Therapeutics have shown the successful application of the latter approach, leading to the identification of MRTX1133 (Figure 1), a highly potent reversible KRAS G12D inhibitor that was
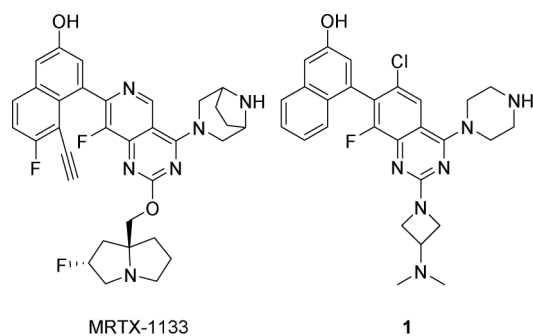

Figure 1. MRTX1133 and early patent hit **1**.

shown to be efficacious in a variety of tumor models.[15,16] However, due to the low oral bioavailability of MRTX1133, *i.p.* dosing was used to establish efficacy and significant formulation work was required to achieve clinically relevant oral exposure. A number of other companies have since reported efforts toward KRAS G12D inhibitors[14,17] or inhibitors that target a number of RAS isoforms.[18−20] Herein we describe the discovery of a highly structurally—distinct series of selective KRAS G12D inhibitors that show promising oral exposure in multiple preclinical species.

RESULTS AND DISCUSSION

Based on the clinical success of KRAS G12C inhibitors and the significant unmet need in tumors driven by the G12D mutation, we initiated a program with the goal of discovering a potent and selective orally bioavailable small molecule inhibitor of KRAS G12D.

At the outset of our program, the feasibility of reversible inhibition of KRAS G12D was still in question. The only available starting points were a peptide developed by Takeda[21,22] and a single example in a patent of a small molecule, compound **1** (Figure 1), related to an earlier G12C lead, where removal of the acrylamide warhead targeting cysteine showed <15 μM potency against KRAS G12D.[23] Therefore, the first goal of the program was to determine if significant potency could be obtained in the absence of a covalent warhead. We elected to use **1** as a point of inquiry for our program.

When tested in house in a biochemical assay measuring the exchange of a fluorescently labeled GDP analog for a nonhydrolyzable analog of GTP in the presence of SOS1, compound **1** showed an IC$_{50}$ of 8 μM. Based on analysis of published KRAS G12C X-ray structures, we hypothesized that the piperazine nitrogen of **1** formed a salt bridge with Asp12, which was subsequently confirmed by researchers at Mirati. Initial SAR focused on optimization of this interaction while holding the rest of the molecule constant. We discovered that introducing a bridge to the piperazine ring (compound **2**, Figure 2) significantly improved potency in the exchange assay, an observation made independently by a number of research groups. With compound **2** in hand, focus shifted to identifying a structurally distinct scaffold. We had reported tricyclic imidazole KRAS G12C inhibitors[24] and hypothesized that a basic amine with a suitable conformational constraint would maintain the key salt bridge with Asp12 in this new scaffold. A preliminary screen of rigid amines identified compound **3** (Figure 2) as a promising hit with an exchange IC$_{50}$ of 671 nM. Compound **3**, like all compounds in this manuscript, contains a stable atropisomeric axis around the core-Switch II bond (highlighted in bold in compound **3**, Figure 2). Unless otherwise stated, potency is reported for the more potent atropisomer.

As we pursued further SAR around compound **3**, it became evident that the azabicyclo[2.2.1]hexane was critical for potency, as virtually all replacements were significantly less active. An X-ray structure of **3** bound to KRAS G12D was solved and suggested a possible explanation for this potency gain (Figure 3A). The protonated amine of the azabicyclo[2.1.1]-hexane formed two key interactions with the protein—a direct hydrogen bond with Tyr96 and a water mediated interaction with Gly10. The rigid bicyclo[2.1.1] hexane structure serves to
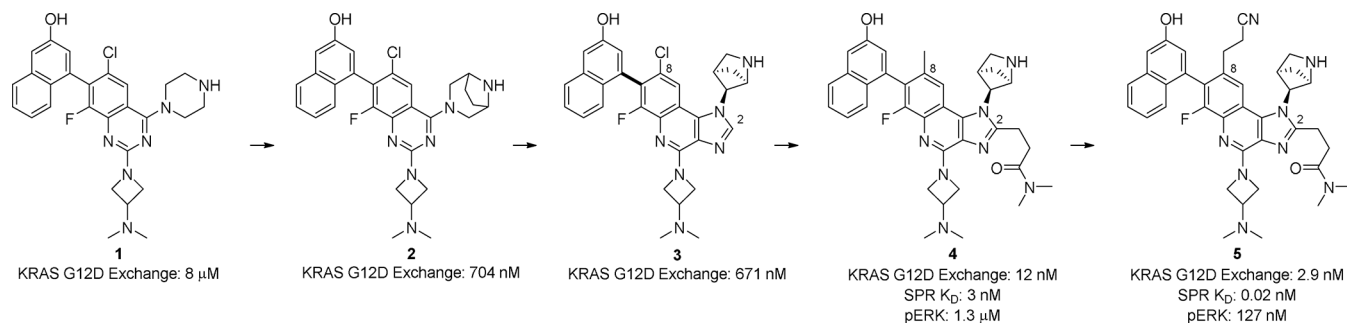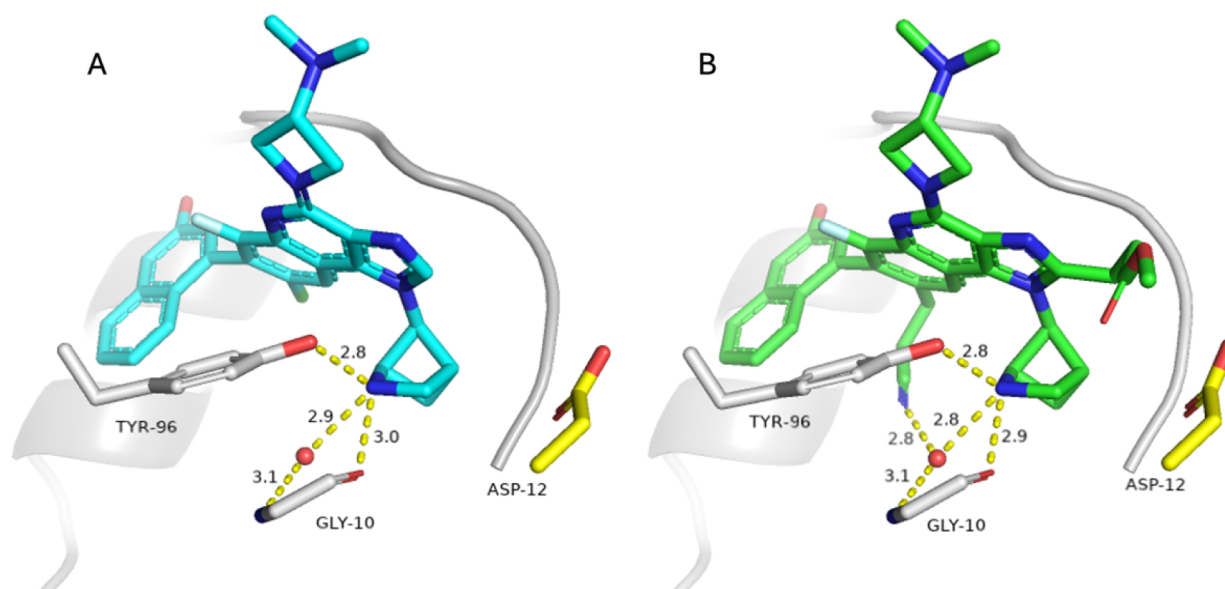

Figure 2. Initial optimization of hit compound **1** to lead compound **5**.

Figure 3. X-ray crystal structure of (A) **3** and (B) **5a** bound to KRAS-G12D (gray). Site of mutation Asp12 is highlighted in yellow. Key interactions for Tyr96 and Gly10 are highlighted with yellow dashed lines and distances (Å). KRAS-G12D bound to **3** and **5a** are deposited in the PDB under PDB ID: 9E5F and 9E5D, respectively.

orient the amine in an otherwise difficult to access conformation directly below the plane of the imidazole core. Contrary to our initial hypothesis, no interactions were made with Asp12, suggesting that additional potency could be realized by growing toward this residue.

Further examination of the X-ray structure identified the imidazole 2 position as a potential vector that could project a substituent toward Asp12 (see Figure 2 for numbering). A two carbon linker between the core and a suitable functionality proved an ideal length, with both shorter and longer chains detrimental to activity. A tertiary amide proved a particularly successful capping group for the linker. In addition, we found that changing chloro to methyl at the 8 position of the tricyclic core provided a ~2 fold improvement in potency. Overall, compound **4** showed a ~50 fold improvement in potency over **3** and also showed cellular potency of 1.3 μM in a homogeneous time-resolved fluorescence (HTRF) assay measuring the phosphorylation of ERK in the KRAS G12D dependent HPAFII cell line.

To further improve potency, we hoped to leverage the structural information available for the Takeda peptide. Published X-ray data showed the peptide binding to an extended conformation of KRAS, in which the Switch II loop opened to reveal a large pocket.[22] Furthermore, multiple reports indicated that the Switch II loop was flexible, adapting a variety of conformations in crystal structures available at the time. We hypothesized that larger substitution in the Switch II region could help to stabilize the Switch II loop in an alternate conformation, opening up an extended pocket in which to gain significant additional potency.

Extensive attempts to do so by substituting various positions on the 3-naphthol severely attenuated potency. The Switch II loop could alternatively be reached by substitution of the core, in particular at the 8 position. Encouraged by preliminary data suggesting that a methyl group showed improved potency relative to chloro (*vide supra*), we also undertook extensive SAR at this vector. Gratifyingly, compound **5** with cyanoethyl substitution increased potency to 2.9 nM, approaching the

lower limit of the exchange assay. Using surface plasmon resonance (SPR) as a more sensitive assay to probe direct binding to KRAS showed that **5** was about 100-fold more potent than **4**. In addition, **5** was the first compound to show potency in an HTRF pERK cell assay in the presence of human whole blood (hWB pERK) below 1 μM (IC$_{50}$ = 977 nM).

An X-ray structure of **5a**, the methyl ester analogue of **5**, was solved to help guide further SAR (Figure 3B). Examination of the structure showed that, contrary to our hypothesis, the Switch II loop was positioned in virtually the same conformation as seen in the X-ray structure of **3**. The cyanoethyl had instead bent underneath the core and made a hydrogen bond with the same water molecule as the azabicyclo[2.1.1]hexane. On the other hand, our hypothesis that growing from the 2 position of the imidazole would yield productive interactions with ASP12 was validated, with the carbonyl forming a hydrogen bond with the backbone N−H. It is notable that, despite not forming a direct hydrogen bond with the Asp12 side chain, compound **5a** maintains significant selectivity over KRAS WT (KRAS G12D SPR: 0.16 nM, KRAS WT SPR: 8.8 nM, 55x selectivity). This level of selectivity was generally maintained when the backbone N−H interaction was present, see Supporting Information for details.

Despite excellent binding potency (20 pM in SPR) compound **5** had relatively poor translation into cellular and whole blood settings, presumably due to a high degree of polarity. In an attempt to attenuate the polarity, we examined the related tricyclic indole core. Cognizant that replacing a nitrogen for a C−H could influence the orientation of the amino azetidine, we surveyed SAR at this position (Table 1), which is pointed toward the solvent front. Indeed, on the indole core the amino azetidine proved inferior to more flexible oxygen linked substituents, in particular the α-methyl pyrrolidinol and a related bicyclic analog first reported by researchers at Mirati.[15] The shift from imidazole to indole had a beneficial effect on cellular translation, though subtle, and the indole core was maintained for subsequent SAR. Ultimately, compound **10** emerged from this

Table 1. Examination of Solvent Front SAR on Indole and Imidazole Cores

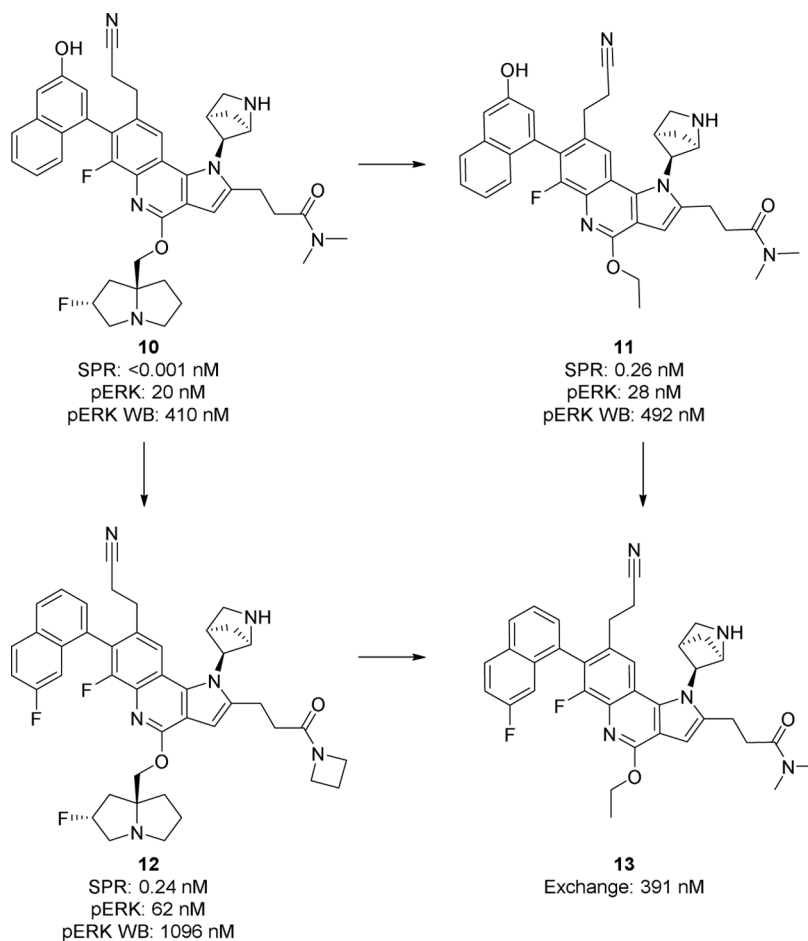| Compound	X	R₁	SPR (nM)	Exc. (nM)	pERK (nM)	hWB pERK (nM)
5	N		0.02	2.9	127	977
6	N		0.031	2.9	92	1241
7	N		N/A	15	1242	N/A
8	C		0.04	3	104	1131
9	C		0.1	3.6	54	2625
10	C		<0.001	2.1	20	410

effort as a new potency record for the program, bottoming out the SPR assay at <1 pM K_d.

Compound **10** represented a key juncture. We had successfully demonstrated that an irreversible warhead was not necessary to achieve excellent potency against the KRAS G12D mutant and that this potency could be achieved with a small molecule. In addition to excellent binding potency, **10** showed 20 nM potency in the pERK cellular assay and <500 nM potency in the hWB pERK assay. However, the path toward a balanced, orally bioavailable compound was not clear. Neither **10** nor any related compounds had any measurable flux in a Caco-2 assay ($<0.1 \times 10^{-6}$ cm/s) and, despite their picomolar binding affinity, showed only moderate translation to a cellular setting, suggesting high polarity. Even with high polarity, **10** and related compounds had high clearance (>1.1 L/h/kg) in human liver microsomes.

In examining the structure of **10**, a number of potential liabilities were identified that we saw as contributing factors to the poor *in vitro* profile.
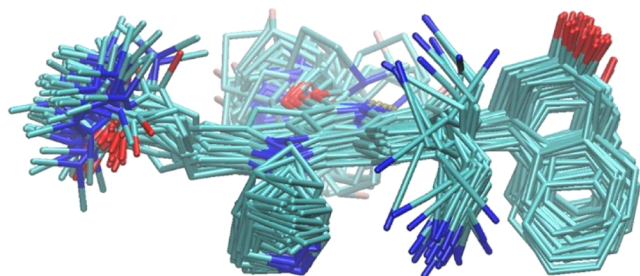
1) Two highly basic amines: the azabicyclo[2.1.1]hexane and the pyrrolidine solvent fragment
2) The hydroxynapthol functionality, a known liability due to glucoronidation and oxidative metabolism[25]
3) Flexibility in the ethyl amide fragment
4) Flexibility in the cyanoethyl fragment

In spite of the detrimental ADME effects, all substituents seemed critical for potency, with each engendering a >10× loss

10
SPR: <0.001 nM
pERK: 20 nM
pERK WB: 410 nM

11
SPR: 0.26 nM
pERK: 28 nM
pERK WB: 492 nM

12
SPR: 0.24 nM
pERK: 62 nM
pERK WB: 1096 nM

13
Exchange: 391 nM

Figure 4. Structural simplification of compound **10**.

Figure 5. Ground state molecular dynamics simulation of compound **10**.

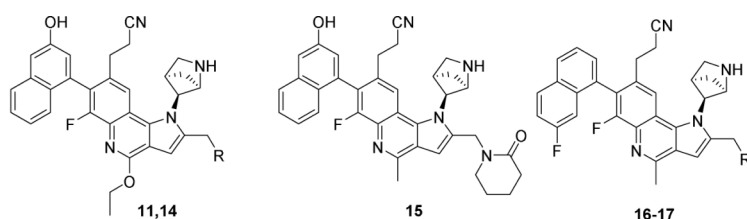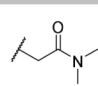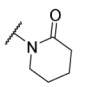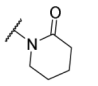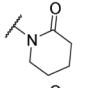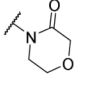in activity if removed. Nevertheless, the team decided that further incremental changes on the current scaffold would not provide oral exposure befitting a developmental candidate and delineated a set of targets we felt were necessary to enter more suitable ADME property space. First, the number of basic amines was capped at one. This meant that the pyrrolidinol in the solvent had to be replaced, since all compounds without the azabicyclo[2.1.1]hexane continued to be inactive (>10 μM in exchange potency). Second, the hydroxyl in the Switch II pocket had to be removed or replaced to avoid the associated metabolic liabilities and extra hydrogen bond donor.

We reasoned that by replacing one of the highly polar substituents with a more balanced one, the loss of binding affinity would be compensated by a concurrent improvement in cellular translation. Extensive screening of the Switch II pocket and solvent region followed. Eventually we were able to show that liabilities 1 or 2 could be addressed independently in a limited number of cases without compromising cellular potency

(Figure 4). Compound **11**, with an ethoxy group replacing the pyrrolidinol and compound **12** with the napthol converted to 7-fluoronaphthyl are representative of the general trends observed. Both were 200 fold less potent in the binding assay, but maintained whole blood pERK potency within 2 fold of compound **10**. However, when the SAR was combined, the resulting compound (**13**) lost >30 fold potency. In addition, compounds **11** and **12**, along with all other compounds with only one target liability removed, did not show an improvement in ADME properties. Even **13** showed only a moderate improvement in clearance (0.7 L/h/kg) and no improvement in permeability. Clearly, an additional potency breakthrough would be necessary to achieve our goal.
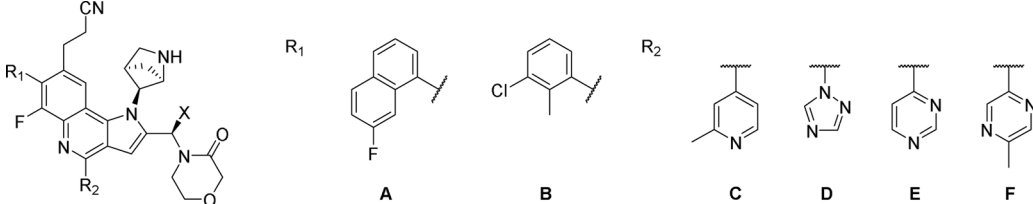
Attention therefore turned to rigidifying the structure. Structural rigidity, as measured by the number of rotatable bonds, has been linked to a number of beneficial properties, from increases in binding potency to improvement in oral bioavailability.[26] As mentioned above, two areas of the molecule with the highest number of rotatable bonds were the cyanoethyl fragment and the amide tail. To evaluate which area was more likely to lead to significant gains we performed 1 μs molecular dynamics simulations on the ground state of a simplified analog of compound **10**. An overlay of all energetically available conformations are shown in Figure 5 and point to the ethyl amide fragment as a significantly more attractive location for additional rigidity. Due to the sterically congested environment around the cyanoethyl, there are two main conformational ensembles observed, with the ensemble containing the largest number of conformations corresponding to the bioactive conformation, which helps explain the significant potency gains realized upon its installation. Conversely, the ethyl amide projects into a sterically unencumbered area and the bioactive conformation represents a small sliver of the overall conformations sampled. It was therefore hypothesized that

Table 2. Mutation Site Cyclization SAR[a]

Compound	R	SPR (nM)	Exc. (nM)	pERK (nM)	hWB pERK (nM)	Caco (cm⁻¹)	h-Cl (L/h/kg)
11		0.26	3.8	28	492	0.2	>1.1
*14**		0.05	2.6	21	2354	0.2	>1.1
15		N/A	3.5	45	597	N/A	N/A
16		N/A	6.1	39	1030	0.7	>1.1
17		N/A	2.7	7.2	677[a]	0.7	>1.1

* Mixture of atropisomers; N/A = not tested; [a] N = 1

[a]All experiments are an average of at least n = 2 unless otherwise noted, see Supporting Information for details.

Table 3. SAR Around Compound 17[a]

Compound	R_1	X	R_2	SPR (nM)	Exc. (nM)	pERK (nM)	hWB pERK (nM)	Caco (cm^{-1})	h-Cl (L/h/kg)
17	A	H	Me	N/A	2.7	7.2	677[b]	0.7	>1.1
18[c]	A	H	C	1.2	6.9	36	565	1.6	1.0
19[c]	A	H	D	0.84	3.7	10	519[b]	1.7	>1.1
20[c]	A	H	E	N/A	3.8	17	626	1.1	0.7
21	A	(R)-Me	C	0.98	2.1	7.5	103	0.6	>1.1
22	A	(R)-Me	F	1.5	2.8	6.8	55	1.4	>1.1
23 (INCB159020)	B	(R)-Me	F	22	4.4	33	331	3.6	1.0

[a]All experiments are an average of at least $n = 2$ unless otherwise noted, see SI for details. [b]$N = 1$. [c]Mixture of atropisomers; N/A = not tested.

Table 4. PK Parameters for Selected Compounds[ab]

Compound	Species	Dose (iv/po)(mg/kg)	C_{max} (nM)	AUC(nM*h)	%F	Cl (%HBF)	$t_{1/2}$ (h)
18	rat	1.0/3.0	41.5	108	11	>100	3.5
18	NHP	0.5/2.0	2.5	BQL	0	37	8.4
22	rat	0.1[c]/3.0	24	85	20	>100	2.5
22	NHP	1.0/20	7.2	68	2	39	4.9
23	rat	1.0/3.0	57	331	27	>100	3.8
23	NHP	1.0/1.5	100	952	42	37	6.4

[a]Full details available in the Supporting Information. [b]BQL = below quantifiable limit. [c]Dose limiting solubity.

locking the ethyl amide in the bioactive conformation would provide larger benefits to potency.

A number of cyclization approaches were attempted, with the goal of keeping a two atom linker between the core and the amide, while keeping the hydroxynaphthyl Switch II piece constant. After significant screening, we discovered that γ-lactam 14 improved potency 5 fold in the binding assay, at the cost of translation to hWB (Table 2). Switching the ethoxy substituent to methyl restored the hWB potency, which proved to be a consistent trend throughout the series.

Gratifyingly, compound 16, with the 3-hydroxynaphthol in 15 replaced with 7-fluoronaphthyl, was the first to maintain WB pERK potency within 2-fold of 10, while meeting both objectives 1 and 2 outlined above. Related compound 17, with an extra oxygen in the mutation site ring, further improved cellular potency to 7.2 nM and hWB potency to 677 nM.

Encouragingly, cyclization improved permeability in the Caco-2 assay (0.7×10^{-6} cm/s). This was the first time permeability was observed in this series, suggesting we had finally identified an appropriate balance of polarity. Indeed, we were able to quickly drive further improvements in properties through examination of the rest of the molecule (Table 3). The solvent was first examined, freed from the requirement of a basic amine. A number of derivatives showed meaningful improvements in permeability while maintaining potency, with compound 18 showing a Caco-2 value of 1.6×10^{-6} cm/s. Similarly, clearance was also beneficially impacted by heteroaryl substitution, with compounds 18 and 20 showing 1.0 and 0.7 L/h/kg, respectively. This was the first time in the program that permeability and clearance could be successfully combined in a single compound (18), validating our hypothesis that only by removing both the hydroxynaphthyl and basic amine in the solvent could we obtain a balanced ADME profile. Encouraged

by in vitro ADME properties, we progressed compounds 18 and 20 into rat PK studies (Table 4). Disappointingly, both compounds showed very high in vivo clearance (>100% hepatic blood flow) and low oral bioavailability (<20%). To ensure that no species specific metabolism issues were present, compound 18 was also dosed in nonhuman primate (NHP). Here the results were mixed. Although oral exposure was below the quantifiable limit, in the i.v. arm, compound 18 showed reasonable clearance (0.97 L/h/kg, 37% hepatic blood flow) and a half-life of 8.4 h.

The complete lack of oral bioavailability in spite of moderate clearance and reasonable permeability in the Caco-2 assay prompted a search for alternative explanations. After extensive profiling, it was discovered that compound 20 suffers significant metabolism in the intestine. In addition, an efflux liability (efflux ratio = 20), albeit saturable at higher concentrations, was observed.

In parallel with the in depth profiling of 18, we continued to conduct SAR to improve the potency and properties of our lead molecule (Table 3). Given the distinct benefit offered by conformational rigidity, we sought to further restrict the degrees of freedom in the morpholinone side chain. To this end, an additional methyl group was introduced at the CH$_2$ linker. We discovered that the (R)-methyl at this position increased potency, with 21, the direct comparator to compound 18, demonstrating a 5 fold improvement of hWB pERK potency, to 100 nM (Table 3). This was the ultimate validation of our search for improved cell translation, as compound 21 had an SPR potency of 0.94 nM, nearly 1000 fold less potent than our starting compound 10, but was more than 5 fold more potent in the hWB pERK assay.

Next, we turned to the ADME properties, in particular permeability, which was limited for 21. Concerned that the

basicity of the 2-methylpyridine was detrimental to properties, we examined less basic diazines. 4-Methylpyrazine in particular possessed a favorable balanced of potency and polarity, with increased permeability (Caco-2 1.4×10^{-6} cm/s) and a further 2 fold boost in potency (compound **22**, Table 3). Compound **22** was dosed in rat and cyno PK, but no improvement in oral bioavailability was observed, despite moderate clearance in the i.v. arm (39% hepatic blood flow).

At this point we shifted our focus to the Switch II pocket 7-fluoronapthalene. While this substituent represented an improvement over the 3-hydroxynapthol fragment, it was still highly electron rich and lipophilic. Extensive screening was undertaken to identify suitable replacements that maintained potency. Naphthyl fragments proved most potent, but we discovered that 2,3-disubstituted phenyl rings could recapitulate a significant amount of the potency while offering clear benefits for properties, presumably due to their decreased lipophilicity and size. 2-Methyl-3-chloro phenyl provided the most balanced compound, **23** (**INCB159020**, Table 3, entry 7). Potency was reduced 3-fold, to 330 nM, but permeability improved greatly (3.6 cm^{-1}) with a moderate improvement in clearance (1.0 L/h/kg). Critically, when dosed orally in NHP at 1.5 mg/kg, we were delighted to see an AUC of 950 nM*hr and oral bioavailability of 42% (Table 4).

A full profile of **23** can be seen in Table 5. Unlike many of the G12C inhibitors, which shows preferential binding to the

Table 5. Full Profile of 23

Assay	Result
KRAS G12D[a] Exc/pERK/CTG Viability	4.4 nM/33 nM/78 nM
WT[b] Exc/pERK/CTG Viability	205 nM/2635 nM/2251 nM (45×)/(80×)/(29×)
Caco-2/h-CI	3.6×10^{-6} cm/s/1.0 L/h/kg
PB (% free)	1.1
Solubility (SGF/FASSIF)	>900 μg/mL/79 μg/mL
CYP[c](3A4/2D6/2C9/2B6/1A2)	17 μM/7.2 μM/>20 μM/>20 μM/>20 μM
hERG[d] IC$_{50}$	11.2 μM
CYP TDI	Clean

[a]Cellular testing performed in HPAFII cells. [b]Cellular testing performed in H838 cells. [c]CYP 3A4 inhibition was measure on the testosterone binding site. [d]hERG manual patch clamp.

inactive GDP state, **23** binds with equal potency to both the active GTP and inactive GDP form as determined by SPR (2.4 nM GDP form, 2.8 nM GTP form). **23** binding was highly selective for KRAS G12D. **23** shows significant selectivity over inhibition of wild-type KRAS, in binding (50× vs binding to KRAS WT), a pERK setting (80 fold selectivity vs a wild-type H838 line) and in a viability setting (28 fold vs a H838 wild-type line). Furthermore, no binding was observed to wild-type HRAS and NRAS in the exchange assay up to a top concentration of 10 μM. A representative 39 kinase panel showed only two kinases with binding <10 μM at 1 mM ATP concentration (TRKA: 3.9 μM, Aurora B: 5.8 μM, full panel data available in the Supporting Information). CYP inhibition was moderate, with an IC$_{50}$ for CYP2D6 most notable at 7.2 μM. hERG channel inhibition was also moderate at 11.2 μM. Given the high degree of protein binding (1.1% free), there was sufficient margin to progress. No time dependent CYP inhibition or PXR activation was observed. Solubility in SGF buffer was excellent at >900 μg/mL, solubility

in FASSIF was lower but still considerable at 79 μg/mL. **23** was therefore progressed to assess *in vivo* activity.

A PK/PD study with **23** was conducted in an HPAC mouse model, which contains ~20−30% WT KRAS stromal cells, limiting maximum inhibition of pERK to ~80%. **23** was administered at a single oral dose of 30, 100 and 300 mg/kg and pERK inhibition was measured at 4 h for the 30 and 100 mg/kg doses and at 24 h for all doses; the MEK inhibitor trametinib was used as positive control (Figure 6). A dose dependent inhibition
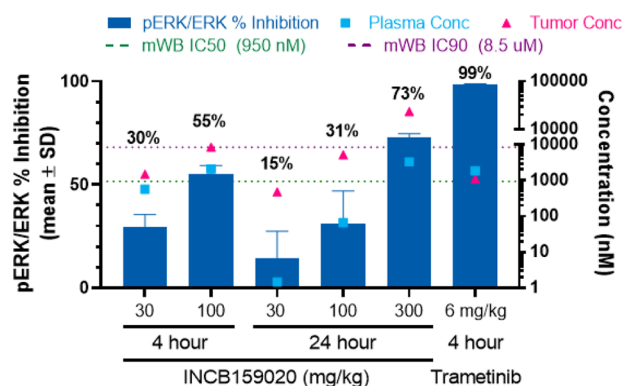

Figure 6. PK/PD evaluation of **23** in mouse HPAC tumors. Trametinib is used as a positive control. HPAC xenografts contain ~20−30% wild-type KRAS stromal content, suggesting maximum G12D related inhibition of 70−80%.

of pERK levels was observed. The 100 mg/kg dose delivered ~70% of maximum inhibition of pERK at 4 h, while the 300 mg/kg dose showed near maximal inhibition out to 24 h post dosing. PK measurements were consistent with this data, with the 100 mg/kg dose displaying plasma concentrations around the mouse WB IC$_{50}$ (950 nM), while the 300 mg/kg dose displayed a plasma concentration near the mouse WB IC$_{90}$ (8.5 μM) at 24 h. **23** was well tolerated at all doses.

Modeling of 23. A model of compound **23** based on accumulated crystallographic data is presented in Figure 7. The key interactions from compounds **3** and **5a** are conserved, with the [2.1.1]bicyclic amine and cyano ethyl group binding a key water and the carbonyl of the morpholinone engaging with the
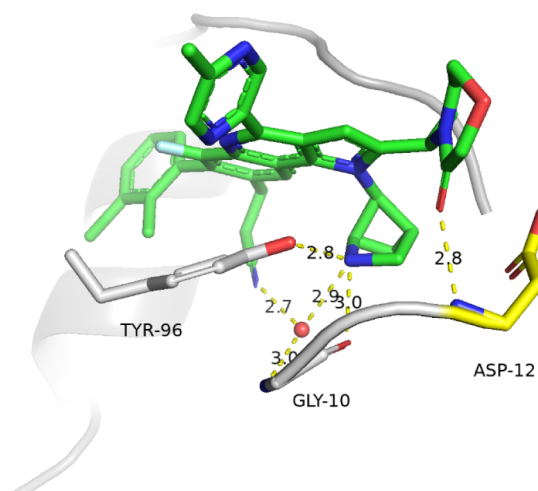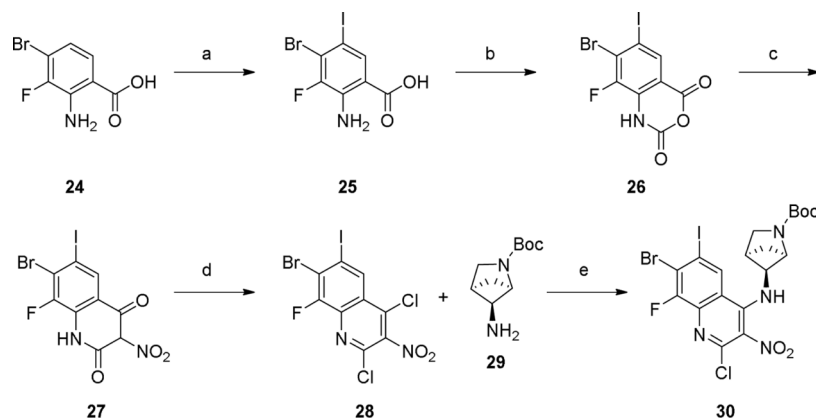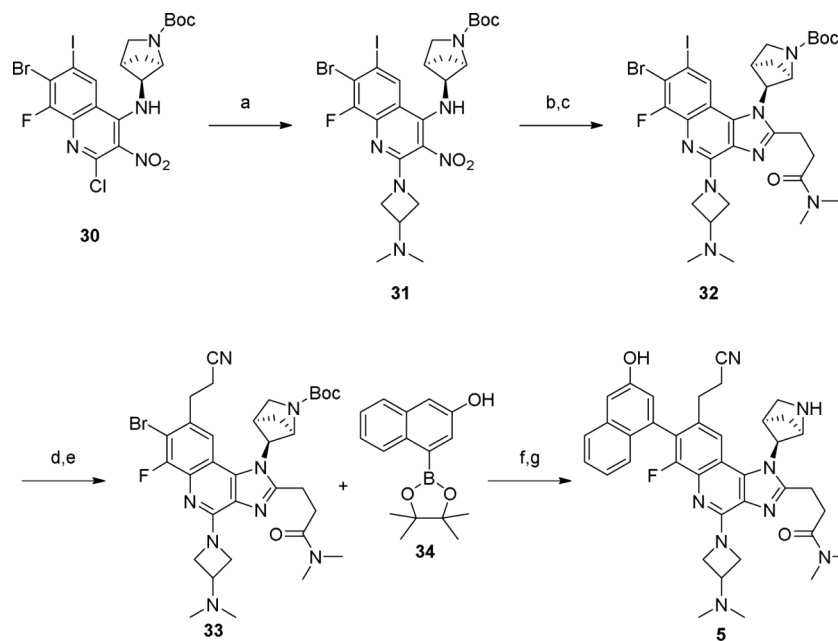

Figure 7. Model of **23** bound to KRAS G12D. Key residues are highlighted. Key interactions are highlighted with yellow dashed lines and distances (Å).

Scheme 1. Synthesis of Key Intermediate 32[a]

[a]Reagents and conditions: (a) NIS, DMF, 60 °C; (b) triphosgene, THF, 60 °C; (c) ethyl nitroacetate, DIPEA, PhMe; (d) POCl₃, DIPEA, 105 °C; (e) DIPEA, NMP, 60 °C.

Scheme 2. Synthesis of Compound 5[a]

[a]Reagents and conditions: (a) 3-dimethylaminoazetidine, 60 °C, NMP; (b) Fe, NH₄Cl, THF/MeOH/H₂O (1:1:1); (c) N,N-dimethyl-4-oxobutanamide, EtOH/AcOH (5:1), 80 °C; (d) acrylonitrile, Pd(OAc)₂, P(o-tol)₃, TEA, DMF, 80 °C; (e) LiEt₃BH, THF, 0 °C; (f) XPhos Pd G2, K₃PO₄, dioxane/water, 80 °C; (g) TFA/DCM (1:1).

backbone N−H of Asp12. The methyl pyrazine is not observed to make any interactions with the protein, although a water mediated interaction can not be ruled out. Importantly, the expected ground state conformation of the side chain closely mimics the bound conformation of ethyl amide of **5a**.

Chemistry. Compounds were generally prepared from a common intermediate **30**, which could be synthesized by the five step sequence outlined in Scheme 1. Thus, iodination of commercially available **24** provided **25**, which was transformed to the dioxine and cyclized with ethyl nitroacetate to provide **27**. Chlorination was followed by immediate displacement with commercial amine **29** to provide **30** as a solid.

Early compounds containing the imidazole core (i.e., **3**−**7**) were prepared according to Scheme 2. The synthesis of compound **5** is shown for reference, full experimental details can be found in the Supporting Information. Installation of the solvent piece could be performed on crude **30** to provide **31**. Reduction of the nitro group was followed by acetic acid-mediated cyclization with the appropriate aldehyde to form the imidazole core. Next, the cyanoethyl fragment was installed via a two step Heck/reduction protocol, providing **33**. Finally, Suzuki cross coupling and deprotection provided compound **5** as a mixture of atropisomers, which could be separated by preparatory HPLC. This strategy was utilized for all compound described below.

The change to the indole core necessitated an alternative synthetic strategy. After investigating a number of routes, we settled on a Sonongashira/cyclization approach. We originally used gold(I) catalysis to achieve the cyclization,[27] but subsequently discovered that reaction profiles were significantly cleaner when an inorganic base (typically cesium carbonate) was used in the absence of transition metal catalysts. The new critical

intermediate thus became **37** (Scheme 3). Thiomethyl was first installed at the 2 position to act as a latent halogen for late stage

Scheme 3. Synthesis of Intermediate 37[a]
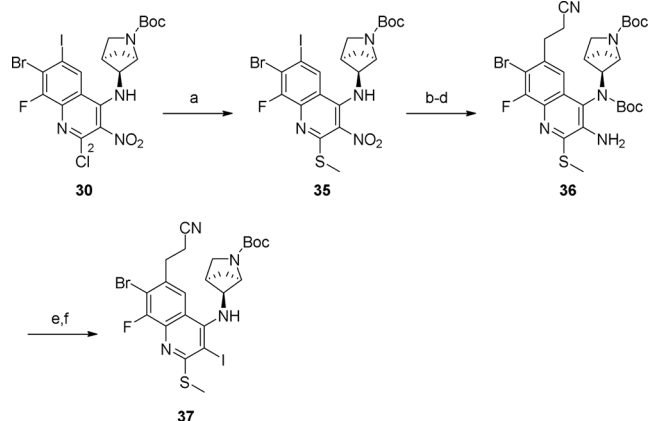
[a]Reagents and conditions: (a) NaSMe, DCM/MeOH (3:1), 0 °C to r.t. (98% from **28**); (b) Boc-anhydride, TEA, DMAP, THF, r.t.; (c) Fe, NH$_4$Cl, THF/MeOH/H$_2$O (1:1:1), 60 °C; (d) Me$_4$NHCO$_2$, Pd(PPh$_3$)$_4$, acrylonitrile, TEA, DMF, 80 °C; (e) NaNO$_2$, H$_2$SO$_4$, KI, CuI, ACN, −15 °C to r.t.; (f) TFA, DCM, then Boc-anhydride, TEA, THF, r.t.

introduction of substitution at this position. The free N−H was then protected to avoid triazole formation during the Sandmeyer reaction. At this stage of the project, we also implemented a one step reductive Heck protocol to reduce the number of synthetic manipulations. Sandmeyer conversion of the amine to the corresponding iodide then proceeded smoothly on the Boc-protected material. Finally, deprotection of both Boc groups simultaneously and reprotection of the basic amine provided intermediate **37**.

Intermediate **37** underwent smooth Sonogashira coupling with a wide variety of alkynes under mild conditions; cyclization was typically performed *in situ* by the addition of cesium

carbonate and heating until full consumption of alkyne was observed (Scheme 4). At this stage the solvent and Switch II pocket piece could be installed interchangeably. In the case of **23**, Suzuki cross coupling was performed first, followed by solvent installation. Heteroatom-linked solvent pieces were typically installed via oxidation to the sulfone and S$_N$Ar displacement, while carbon-linked groups were installed via a Liebskind-Srogl[28,29] reaction with the corresponding boronate or stannyl heterocycle. Finally, Suzuki cross coupling and deprotection provided final compounds. The synthesis of **23** is shown in Scheme 4, synthetic procedures for other compounds can be found in the experimental section of the Supporting Information. The synthesis of alkyne **38** is shown in Scheme 5. (*R*)-butynamine was reacted with 2-(2-chloroethoxy)acetyl chloride, then cyclized under basic conditions.

**Scheme 5. Synthesis of Alkyne 40**[a]
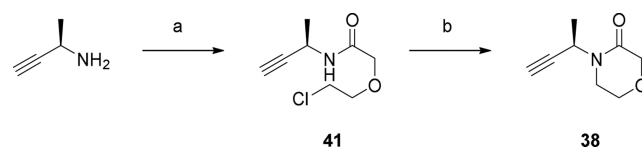
[a]Reagents and conditions: (a) 2-(2-chloroethoxy)acetyl chloride, TEA, THF, r.t.; (b) NaH, THF, r.t.

◼ CONCLUSION

In summary, we demonstrate the discovery of a potent and selective KRAS G12D inhibitor with promising target engagement *in vivo*. Due to uncertainties about the druggability of KRAS G12D, we utilized a two-step strategy. First, proof of concept for potent inhibition of KRAS G12D was achieved by focusing on identifying additional interactions with the protein. Second, we were able to balance the delicate interplay of potency and bioavailability by identifying key structural features interfering with oral exposure, removing them despite the significant loss of binding affinity, then building potency back

Scheme 4. Synthesis of Compound 23[a]
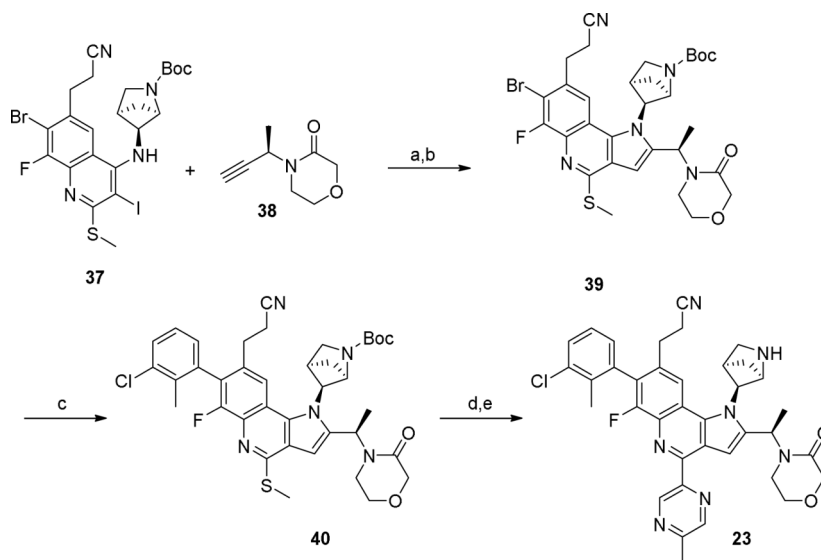
[a]Reagents and conditions: (a) CuI, (PPh$_3$)$_4$Pd, TEA, DMF, 70 °C; (b) Cs$_2$CO$_3$, DMF, 70 °C; (c) (3-chloro-2-methylphenyl)boronic acid, (PPh$_3$)$_4$Pd, K$_3$PO$_4$, dioxane/water (4:1), 80 °C; (d) (PPh$_3$)$_4$Pd, Cu(3-methylsalicylate), dioxane, 120 °C; (e) TFA/DCM (1:1).

with a focus on properties. Rigidifying the structure proved key in this endeavor, increasing potency by reducing the degrees of freedom while simultaneously improving ADME. These changes allowed for promising oral exposure and bioavailabiliy in multiple preclinical species. The resulting compound **23** (**INCB159020**) serves as an important tool compound and provides a framework for the design of future bioavailable KRAS inhibitors.

■ EXPERIMENTAL SECTION

General Information. Unless otherwise specified, all solvents were purchased from commercial sources and used without further drying. Column chromatography was performed using prepackaged columns (RediSep Rf or SNAP) using Biotage Isolera or Teledyne ISCO CombiFlash system. NMR spectra were obtained using a Varian Mercury-400, Inova-500, or a Bruker Advance III HD 600 MHz spectrometer equipped with a 5 mm QCI Cryoprobe. Data for ^{1}H spectra are reported as follows: chemical shift (δ ppm), multiplicity, coupling constant (Hz), integration and are referenced to the residual solvent peak (2.50 for DMSO-d_6 and 7.26 ppm for CDCl$_3$). Data for ^{13}C spectra are reported as follows: chemical shift (δ ppm), multiplicity, coupling constant (Hz) and are referenced to the residual solvent peak (40 ppm for DMSO-d_6) and are proton decoupled. Preparative LC purifications were performed on a Waters FractionLynx system using UV-triggered or mass directed fractionation and compound-specific method optimization. For purification of final compounds, the reaction mixture was diluted with methanol or acetonitrile to 6 mL total volume, and then filtered through a syringe filter. Purification was then performed with prep-LCMS with the following general conditions: XBridge C18 column, gradient of acetonitrile/water containing 0.1% TFA, flow rate of 60 mL/min. Unless otherwise indicated, compounds were isolated as the corresponding TFA salt. All final compounds for biological testing were purified by reverse phase prep-HPLC to >95% purity as determined by analytical HPLC.

Synthesis of **23**. *Step 1. 2-Amino-4-bromo-3-fluoro-5-iodobenzoic acid (25).* NIS (21.15 g, 94 mmol) was added to a solution of 2-amino-4-bromo-3-fluorobenzoic acid (20 g, 85 mmol) in DMF (200 mL) and the reaction was stirred at 80 °C for 3 h. The mixture was cooled with ice water and then water (500 mL) was added, the precipitate was filtered, washed with water and dried to provide the desired product as a solid. The crude solid was used in the next step without further purification. LC-MS calculated for C$_7$H$_5$BrFINO$_2^+$ (M + H)$^+$: m/z = 359.9, 361.9; found 359.9, 361.9.

Step 2. 7-Bromo-8-fluoro-6-iodo-2H-benzo[d][1,3]-oxazine-2,4(1H)-dione (26). Triphosgene (9.07 g, 30.6 mmol) was added to a solution of **25** (22 g, 61.1 mmol) in dioxane (200 mL) and the reaction was stirred at 80 °C for 2 h. The reaction mixture was cooled with ice water and then filtered. The solid was washed with ethyl acetate to provide the desired product as a solid. The crude product was used in the next step without further purification. LC-MS calculated for C$_8$H$_3$BrFINO$_3^+$ (M + H)$^+$: m/z = 385.8, 387.8; found 385.8, 387.8.

Step 3. 7-Bromo-8-fluoro-6-iodo-3-nitroquinoline-2,4-diol (27). DIPEA (25.5 mL, 146 mmol) was added to a solution of ethyl 2-nitroacetate (16.33 mL, 146 mmol) and **26** (20 g, 73.0 mmol) in toluene (200 mL) at r.t. The reaction was stirred at 95 °C for 3 h. The reaction was cooled and then filtered, the solid was washed with a small amount of hexanes to provide the

desired product. The crude product was used in the next step without further purification. LC-MS calculated for C$_9$H$_4$BrFIN$_2$O$_4^+$ (M + H)$^+$: m/z = 428.8, 430.8; found 428.8, 430.8.

Step 4. 7-Bromo-2,4-dichloro-8-fluoro-6-iodo-3-nitroquinoline (28). DIPEA (8.14 mL, 46.6 mmol) was added to a mixture of **27** (10 g, 23.31 mmol) in POCl$_3$ (10.86 mL, 117 mmol). The reaction mixture was stirred at 100 °C for 2 h. The solvent was removed under vacuum and then azeotroped with toluene 3 times to provide the crude material which was purified with flash column chromatography (0−100% ethyl acetate in hexanes) to provide the desired product. LC-MS calculated for C$_9$H$_2$BrCl$_2$FIN$_2$O$_2^+$ (M + H)$^+$: m/z = 464.8, 466.8; found 464.8, 466.8.

Step 5. tert-Butyl (1R,4R,5S)-5-((7-Bromo-8-fluoro-6-iodo-2-(methylthio)-3-nitroquinolin-4-yl)amino)-2-azabicyclo[2.1.1]hexane-2-carboxylate (35). To a solution of **28** (220.6 g, 474 mmol) and *tert*-butyl (1R,4R,5S)-5-amino-2-azabicyclo[2.1.1]hexane-2-carboxylate (96 g, 483 mmol) in DMF (600 mL) was added Hunig's base (103 mL, 592 mmol) and the reaction mixture was heated to 60 °C for 1 h. The reaction mixture was then cooled to 0 °C in an ice bath and sodium thiomethoxide (100 g, 1421 mmol) and MeOH (100 mL) were added. The mixture was stirred at 0 °C for 1 h, then poured into ice water. The resulting precipitate was filtered, washed with ice water, then dried under vacuum to afford the desired product (297.6 g, 98%). LC-MS calculated for C$_{20}$H$_{22}$BrFIN$_4$O$_4$S$^+$ (M + H)$^+$: m/z = 639.0; found 639.1.

Step 6. tert-Butyl (1R,4R,5S)-5-((7-Bromo-8-fluoro-6-iodo-2-(methylthio)-3-nitroquinolin-4-yl)(tert-butoxycarbonyl)-amino)-2-azabicyclo[2.1.1]hexane-2-carboxylate. To a solution of **35** (272 g, 425 mmol) in THF (850 mL) was added triethylamine (267 mL, 1.9 mol), DMAP (5.2 g, 42.5 mmol), and di-*tert*-butyl dicarbonate (334 g, 1.5 mol) sequentially at room temperature, and the reaction mixture was heated to 50 °C for 3 h. The reaction mixture was diluted with EtOAc and washed with saturated NaHCO$_3$ and brine. The organic layer was dried over MgSO$_4$, filtered, and concentrated. The product was used without purification. LC-MS calculated for C$_{21}$H$_{22}$BrFIN$_4$O$_6$S$^+$ (M + H−C$_4$H$_8$)$^+$: m/z = 683.0; found 683.1.

Step 7. tert-Butyl (1R,4R,5S)-5-((3-Amino-7-bromo-8-fluoro-6-iodo-2-(methylthio)quinolin-4-yl)(tert-butoxycarbonyl)-amino)-2-azabicyclo[2.1.1]hexane-2-carboxylate. A 2-L flask equipped with a mechanical stirrer was charged with the product from the previous step (283.7 g, 384 mmol), MeOH (320 mL), water (320 mL), and THF (320 mL). Iron (214 g, 3.84 mol) and ammonium chloride (215 g, 4 mol) were added, and the reaction mixture was stirred at 60 °C for 2 h. The reaction mixture was diluted with EtOAc and filtered through a pad of Celite. The layers were separated and the organic layer was washed with brine, dried over MgSO$_4$, filtered and concentrated. The product was used without purification (250 g, > 99%). LC-MS calculated for C$_{25}$H$_{32}$BrFIN$_4$O$_4$S$^+$ (M + H)$^+$: m/z = 709.0; found 709.1.

Step 8. tert-Butyl (1R,4R,5S)-5-((3-Amino-7-bromo-8-fluoro-6-iodo-2-(methylthio)quinolin-4-yl)(tert-butoxycarbonyl)-amino)-2-azabicyclo[2.1.1]hexane-2-carboxylate (36). To a solution of the product from the previous step (51 g, 78 mmol) in DMF (200 mL) were added acrylonitrile (103 mL, 1.56 mol), tetramethylammonium formate (60.8 mL, 156 mmol) and DIPEA (27.3 mL, 156 mmol), followed by tetrakistriphenylphosphine palladium (20.3 g, 17.56 mmol). The reaction flask was evacuated, backfilled with nitrogen, then stirred under a

nitrogen atmosphere at 50 °C overnight. The reaction was quenched with water and extracted with ethyl acetate. The organic layer was washed with water and brine, dried over sodium sulfate and concentrated. The crude product was purified by silica gel chromatography (0−100% hexanes/ethyl acetate) to provide the desired product (18.1 g, 36% over 3 steps). LC-MS calculated for $C_{28}H_{36}BrFN_5O_4S^+$ $(M + H)^+$: m/z = 636.2; found 636.3.

Step 9. tert-Butyl (1R,4R,5S)-5-((7-Bromo-6-(2-cyanoethyl)-8-fluoro-3-iodo-2-(methylthio)quinolin-4-yl)amino)-2-azabicyclo[2.1.1]hexane-2-carboxylate (37). To a solution of **36** (22 g, 34.6 mmol) in acetonitrile (135 mL) at −20 °C was added a solution of sulfuric acid (4.61 mL, 86 mmol) in water (3 mL). A solution of sodium nitrite (4.77 g, 69.1 mmol) in a minimum amount of water was next added dropwise, maintaining the temperature of the reaction mixture around −20 °C. After addition was complete, the reaction mixture was stirred at −10 °C for 5 min, then a concentrated solution of potassium iodide (22.95 g, 138 mmol) in water was added slowly, maintaining reaction temperature around −20 °C. After addition was complete, the reaction mixture was stirred at −10 °C for 45 min, then quenched with sat. sodium thiosulfate and extracted with ethyl acetate. The organic layer was washed with sat. sodium bicarbonate, sat. sodium thiosulfate, water and brine, dried over sodium sulfate and concentrated. The crude product was dissolved in DCM/TFA (1:1, 150 mL) and stirred at r.t. for 3 h, then concentrated and azeotroped with acetonitrile three times. The residue was dissolved in THF (150 mL) and triethylamine (48.2 mL, 346 mmol) and boc-anhydride (7.54 g, 34.6 mmol) were added. The reaction mixture was stirred at r.t. for 1 h, then quenched with water and extracted with ethyl acetate. The organic layer was washed with water and brine, dried over sodium sulfate and concentrated. The product was purified by FCC (0−50% EtOAc/hexanes) to yield the title compound (10.7 g, 48% over 3 steps). LC-MS calculated for $C_{23}H_{26}BrFIN_4O_2S^+$ $(M + H)^+$: m/z = 647.0; found 647.0.

Step 10. tert-Butyl (1R,4R,5S)-5-(7-Bromo-8-(2-cyanoethyl)-6-fluoro-4-(methylthio)-2-((R)-1-(3-oxomorpholino)-ethyl)-1H-pyrrolo[3,2-c]quinolin-1-yl)-2-azabicyclo[2.1.1]-hexane-2-carboxylate (39). A solution of **37** (3.6 g, 5.56 mmol), **38** (1.70 g, 11.12 mmol, see Supporting Information), DIPEA (9.7 mL, 55.6 mmol), Pd(PPh₃)₄ (1.28 g, 1.11 mmol), and copper(I) iodide (0.424 g, 2.22 mmol) in DMF (55 mL) was stirred at 70 °C for 1 h. Sat. aq. ammonium chloride was then added and the mixture was extracted with ethyl acetate. The organic layer was washed with water and brine, dried over sodium sulfate and concentrated. The crude product was dissolved in DMF (55 mL) and cesium carbonate (5.38 g, 16.5 mmol) was added and heating was continued at 70 °C for 1 h. The reaction was quenched with a small amount of concentrated aq. ammonium hydroxide, diluted with water and extracted with ethyl acetate. The organic layer was washed with water and brine, dried over sodium sulfate and concentrated. The crude product was purified by flash column chromatography (0−100% ethyl acetate in DCM) to provide the desired product (3.25 g, 88%). LC-MS calculated for $C_{31}H_{36}BrFN_5O_4S^+$ $(M + H)^+$: m/z = 672.2; found 672.2.

Step 11. tert-Butyl (1R,4R,5S)-5-(7-(3-Chloro-2-methyl-phenyl)-8-(2-cyanoethyl)-6-fluoro-4-(methylthio)-2-((R)-1-(3-oxomorpholino)ethyl)-1H-pyrrolo[3,2-c]quinolin-1-yl)-2-azabicyclo[2.1.1]hexane-2-carboxylate (40). A solution of **39** (2.16 g, 3.21 mmol), (3-chloro-2-methylphenyl)boronic acid (1.09 g, 6.42 mmol), Pd(PPh₃)₄ (0.742 g, 0.642 mmol) and

potassium phosphate (1.70 g, 8.03 mmol) in 1,4-dioxane (20 mL) and water (4 mL) was stirred at 80 °C for 30 min. The reaction was then concentrated and purified by flash chromatography (0−100% ethyl acetate in hexanes) to afford the title compound (1.36 g, 59%). LC-MS calculated for $C_{38}H_{42}ClFN_5O_4S^+$ $(M + H)^+$: m/z = 718.3; found 718.3.

Step 12. 3-(1-((1R,4R,5S)-2-Azabicyclo[2.1.1]hexan-5-yl)-7-(3-chloro-2-methylphenyl)-6-fluoro-4-(5-methylpyrazin-2-yl)-2-((R)-1-(3-oxomorpholino)ethyl)-1H-pyrrolo[3,2-c]-quinolin-8-yl)propanenitrile (23). A solution of **40** (1.25 g, 1.74 mmol), Pd(PPh₃)₄ (1.00 g, 0.870 mmol), copper(I) 3-methylsalicylate (1.87 g, 8.70 mmol) and 2-methyl-5-(4,4,5,5-tetramethyl-1,3,2-dioxaborolan-2-yl)pyrazine (1.92 g, 8.70 mmol) in 1,4-dioxane (10 mL) was stirred at 120 °C for 1 h. The reaction mixture was filtered through a thiol SiliaPrep SPE cartridge and concentrated. The residue was stirred in 1:1 DCM/TFA (30 mL) for 30 min, concentrated and purified by prep HPLC (pH 2). LC-MS calculated for $C_{37}H_{36}ClFN_7O_2^+$ $(M + H)^+$: m/z = 664.3; found 664.4. ^1H NMR (500 MHz, DMF-d_7) δ 9.71 (d, J = 1.5 Hz, 1H), 8.81 (d, J = 1.5 Hz, 1H), 8.63 (s, 1H), 7.84 (s, 1H), 7.65 (m, 1H), 7.49 (m, 2H), 6.38 (q, J = 6.3 Hz, 1H), 5.07 (m, 1H), 4.63 (d, J = 5.9 Hz, 1H), 4.21 (d, J = 16.5 Hz, 1H), 4.16 (d, J = 16.5 Hz, 1H), 3.82 (m, 1H), 3.76 (m, 1H), 3.59 (m, 1H), 3.12 (m, 1H), 3.10 (m, 1H), 2.96 (m, 2H), 2.91 (m, 1H), 2.67 (s, 3H), 2.60 (m, 1H), 2.52 (d, J = 8.6 Hz, 1H), 2.19 (s, 3H), 1.94 (d, J = 7.0 Hz, 1H), 1.69 (d, J = 6.7 Hz, 3H), 1.36 (d, J = 8.6 Hz, 1H), 1.22 (d, J = 7.0 Hz, 1H).

Synthesis of 5. Step 1. tert-Butyl (1R,4R,5S)-5-((7-Bromo-2-(3-(dimethylamino)azetidin-1-yl)-8-fluoro-6-iodo-3-nitro-quinolin-4-yl)amino)-2-azabicyclo[2.1.1]hexane-2-carboxylate (31). To a mixture of **28** (4.0 g, 8.59 mmol) in CH_2Cl_2 (60 mL) was added *tert*-butyl (1R,4R,5S)-5-amino-2-azabicyclo-[2.1.1]hexane-2−20 carboxylate (1.7 g, 8.59 mmol) and DIPEA (7.48 mL, 42.9 mmol) and the reaction was stirred at 55 °C for 4 h. Then N,N-dimethylazetidin-3-amine dihydrochloride (1.63 g, 9.45 mmol) was added. After heating at 55 °C for another 4 h, the mixture was concentrated to dryness, and used without further purification (5.0 g, 84%). LCMS calculated for $C_{24}H_{30}BrFIN_6O_4$ $(M + H)+$: m/z = 691.1; found 691.2.

Step 2. tert-Butyl (1R,4R,5S)-5-((3-Amino-7-bromo-2-(3-(dimethylamino)azetidin-1-yl)-8-fluoro-6-iodoquinolin-4-yl)amino)-2-azabicyclo[2.1.1]hexane-2-carboxylate. Sodium hydrosulfite (2.86 g, 16.4 mmol) in water (2.5 mL) was added to a solution of **33** (2.27 g, 3.28 mmol) and 30% aq. ammonium hydroxide (4.26 mL, 32.8 mmol) in MeOH (30 mL) at 0 °C. After 10 min, water (30 mL) was added to the reaction mixture followed by extraction with dichloromethane (30 mL × 3). The combined organic layers were dried Na_2SO_4, filtered and concentrated. The crude product was added to a silica gel column and was eluted with methanol/dichloromethane from 0% to 10% to provide the desired product (1.9 g, 88% yield). LCMS calculated for $C_{24}H_{32}BrFIN_6O_2$ $(M + H)+$: m/z = 661.1; found 661.2.

Step 3. tert-Butyl (1R,4R,5S)-5-(7-Bromo-2-(3-(dimethyla-mino)-3-oxopropyl)-4-(3-(dimethylamino)azetidin-1-yl)-6-fluoro-8-iodo-1H-imidazo[4,5-c]quinolin-1-yl)-2-azabicyclo-[2.1.1]hexane-2-carboxylate (32). A solution of the product above (3.00 g, 4.54 mmol) and N,N-dimethyl-4-oxobutanamide (0.615 g, 4.76 mmol) in ethanol (9.1 mL) was heated to 85 °C in a sealed vial under air for 3 h. The vial was cooled to 22 °C and *n*-butanol (9 mL) was added, the vial uncapped, and the mixture stirred vigorously overnight (open to air) at 65 °C. Volatiles were removed in vacuo and the product was used without

further purification (>99%). LCMS calculated for $C_{30}H_{39}BrFIN_7O_3$ (M + H)+: m/z = 770.1; found: 770.1.

Step 4. tert-Butyl (1R,4R,5S)-5-(7-Bromo-8-(2-cyanoethyl)-2-(3-(dimethylamino)-3-oxopropyl)-4-(3-(dimethylamino)-azetidin-1-yl)-6-fluoro-1H-imidazo[4,5-c]quinolin-1-yl)-2-azabicyclo[2.1.1]hexane-2-carboxylate (33). In a 40 mL vial, **32** (3.50 g, 4.54 mmol) and bis(tri-*o*-tolylphosphine)palladium-(0) (0.325 g, 0.454 mmol) were dissolved in DMF (15 mL). Triethylamine (1.266 mL, 9.09 mmol) and acrylonitrile (0.598 mL, 9.09 mmol) were added to the reaction mixture. The headspace was purged with nitrogen and the vial was capped and stirred at 80 °C for 1 h. The reaction mixture was cooled to r.t and poured into rapidly stirring ice water to precipitate a yellow solid. The solid was filtered and dried on the filter for 72 h. The crude solid was dissolved in THF (40 mL) and cooled to 0 °C. Lithium triethylborohydride (8.2 mL, 1 M in THF, 1.81 equiv) was added in four portions over 30 min with LCMS monitoring after each addition. Water was slowly added to the reaction mixture (20 mL) and the mixture was extracted with DCM (3 × 20 mL), dried over MgSO$_4$, and volatiles removed *in vacuo* to provide the desired product (3.24 g, quant.). LCMS calculated for $C_{33}H_{43}BrFN_8O_3$ (M + H)+: m/z = 697.3; found: 697.4.

Step 5. 3-(1-((1R,4R,5S)-2-Azabicyclo[2.1.1]hexan-5-yl)-8-(2-cyanoethyl)-4-(3-(dimethylamino)azetidin-1-yl)-6-fluoro-7-(3-hydroxynaphthalen-1-yl)-1H-imidazo[4,5-c]quinolin-2-yl)-N,N-dimethylpropanamide (5). A mixture of **33** (900 mg, 1.29 mmol), **34** (419 mg, 1.55 mmol), XPhos Pd G2 (51 mg, 0.065 mmol) and K$_3$PO$_4$ (551 mg, 2.59 mmol) in dioxane/water (4:1, 5 mL) was heated to 100 °C for 2 h. The reaction mixture was quenched with water and extracted with ethyl acetate. The organic layer was washed with water and brine, dried over sodium sulfate and concentrated. The crude product was dissolved in 1:1 DCM/TFA (6 mL) and stirred at r.t. for 30 min, then diluted with acetonitrile and purified by reverse-phase HPLC (pH 2) to provide the desired product. LCMS calculated for $C_{38}H_{42}FN_8O_2$ (M + H)+: m/z = 660.3; found: 660.2. ^{1}H NMR (600 MHz, DMSO-d_6) δ 10.16 (s, 1H), 8.04 (s, 1H), 7.82–7.73 (m, 1H), 7.45–7.36 (m, 1H), 7.24 (s, 1H), 7.18–7.13 (m, 1H), 7.12–7.05 (m, 2H), 4.75 (s, 1H), 4.51–4.34 (m, 2H), 4.34–4.30 (m, 1H), 4.20–4.05 (m, 2H), 3.63–3.48 (m, 1H), 3.26–3.13 (m, 3H), 3.06 (s, 3H), 2.96–2.85 (m, 2H), 2.84 (s, 3H), 2.76–2.67 (m, 1H), 2.64–2.55 (m, 4H), 2.14 (s, 6H), 1.92–1.85 (m, 1H), 1.29–1.18 (m, 2H). ^{13}C NMR (126 MHz, DMSO) δ 166.9, 155.7, 154.4, 149.4, 148.6, 143.8, 143.6, 142.9, 140.7, 137.2, 135.7, 135.2, 134.9, 134.8, 133.1, 129.9, 129.5, 128.1, 125.2, 120.6, 119.9, 119.1, 118.5, 109.4, 67.7, 63.9, 60.6, 58.1, 46.4, 44.9, 43.6, 40.7, 30.4, 28.8, 21.6, 17.6, 17.5, 16.3

*Synthesis of Compound **16**. Step 1. tert-Butyl (1R,4R,5S)-5-((7-Bromo-6-(2-cyanoethyl)-8-fluoro-2-(methylthio)-3-(3-(2-oxopiperidin-1-yl)prop-1-yn-1-yl)quinolin-4-Yl)amino)-2-azabicyclo[2.1.1]hexane-2-carboxylate (42).* To a mixture of **37** (590 mg, 0.91 mmol), copper iodide (69 mg, 0.36 mmol) and Pd(PPh$_3$)$_4$ (211 mg, 0.18 mmol) were added DMF (3 mL), Hunig's base (0.8 mL, 4.56 mmol) and 1-(prop-2-yn-1-yl)piperdin-2-one (250 mg, 1.82 mmol). The reaction was sparged with nitrogen, then stirred at 70 °C for 2 h, then quenched with a small amount of sat. aq. ammonium hydroxide. The mixture was diluted with water and extracted with ethyl acetate. The organic layer was washed with water and brine, dried over sodium sulfate and concentrated. The crude product was purified by column chromatography (0–100% ethyl acetate in heptane) to provide the desired product (335 mg, 56%).

LCMS calculated for $C_{31}H_{36}BrFN_5O_3S$ (M + H)$^+$: m/z = 656.2, 658.2; Found: 656.2, 658.2.

Step 2. tert-Butyl (1R,4R,5S)-5-(7-Bromo-8-(2-cyanoethyl)-6-fluoro-4-(methylthio)-2-((2-oxopiperidin-1-yl)methyl)-1H-pyrrolo[3,2-c]quinolin-1-Yl)-2-azabicyclo[2.1.1]hexane-2-carboxylate (43). To a solution of **42** (335 mg, 0.51 mmol) in THF (5 mL) were added IPrAuCl (63 mg, 0.10 mmol) and silver tetrafluoroborate (149 mg, 0.76 mmol) and the reaction mixture was stirred at 70 °C under nitrogen for 2 h. ~10−20% Boc loss was observed by LCMS, so triethylamine (36 μL and boc-anhydride (223 mg, 1.02 mmol) were added. After 30 min, the reaction was quenched with brine and extracted with ethyl acetate. The organic layer was washed with sat. aqueous ammonium hydroxide, dried over magnesium sulfate and concentrated. The crude product was purified by flash column chromatography (0−100% ethyl acetate in heptane) to provide the desired product (253 mg, 75%). LCMS calculated for $C_{31}H_{36}BrFN_5O_3S$ (M + H)$^+$: m/z = 656.2, 658.2; Found: 656.2, 658.2.

Step 3. tert-Butyl (1R,4R,5S)-5-(7-Bromo-8-(2-cyanoethyl)-6-fluoro-4-(methylsulfinyl)-2-((2-oxopiperidin-1-yl)methyl)-1H-pyrrolo[3,2-c]quinolin-1-yl)-2-azabicyclo[2.1.1]hexane-2-carboxylate (44). To a solution of **43** (253 mg, 0.385 mmol) in DCM (2.5 mL) at 0 °C was added *m*-CPBA (86 mg, 0.385 mmol) and the reaction mixture was stirred at this temperature for 30 min. The reaction was quenched with sat. sodium thiosulfate and extracted with DCM. The organic layer was washed with brine, dried over sodium sulfate and concentrated. The crude product was purified by column chromatography (0−100% ethyl acetate in hexanes) to provide the desired product. LCMS calculated for $C_{31}H_{36}BrFN_5O_4S$ (M + H)$^+$: m/z = 672.2, 674.2; Found: 672.2, 674.2.

Step 4. tert-Butyl (1R,4R,5S)-5-(7-Bromo-8-(2-cyanoethyl)-6-fluoro-4-methyl-2-((2-oxopiperidin-1-yl)methyl)-1H-pyrrolo[3,2-c]quinolin-1-yl)-2-azabicyclo[2.1.1]hexane-2-carboxylate (45). To a solution of **44** (311 mg, 0.46 mmol) in THF (2.5 mL) at 0 °C was added MeMgBr (3 M in THF, 385 μL, 1.16 mmol) dropwise and the reaction mixture was stirred at r.t. for 30 min, then quenched with sat. ammonium chloride and extracted with ethyl acetate. The organic layer was washed with water and brine, dried over sodium sulfate and concentrated. The crude product was purified by flash chromatography (0−100% ethyl acetate in hexanes) to provide the desired product. LCMS calculated for $C_{31}H_{36}BrFN_5O_3$ (M + H)$^+$: m/z = 624.2, 626.2; Found: 624.2, 626.2.

Step 5. 3-(1-((1R,4R,5S)-2-Azabicyclo[2.1.1]hexan-5-yl)-6-fluoro-7-(7-fluoronaphthalen-1-yl)-4-methyl-2-((2-oxopiperidin-1-yl)methyl)-1H-Pyrrolo[3,2-c]quinolin-8-yl)-propanenitrile (16). To a mixture of **45** (29 mg, 0.038 mmol), 2-(7-fluoronaphthalen-1-yl)-4,4,5,5-tetramethyl-1,3,2-dioxaborolane (22 mg, 0.76 mmol), XPhos Pd G2 (6 mg, 7.6 μmol) and potassium phosphate, tribasic (24 mg, 0.11 mmol) were added dioxane/water (4:1, 1 mL) and the reaction was sparged with nitrogen, then stirred at 80 °C for 1 h. The reaction was quenched with water and extracted with ethyl acetate. The organic layer was washed with water and brine, dried over sodium sulfate and concentrated. The crude product was dissolved in 1:1 DCM/TFA (1 mL) and stirred at r.t. for 15 min, then diluted with MeOH and purified by prep-LCMS (XBridge C18 column, eluting with a gradient of acetonitrile/water containing 0.1% TFA, at flow rate of 60 mL/min) to afford the desired product. LCMS calculated for $C_{37}H_{36}F_2N_5O_2$ (M + H)$^+$: m/z = 620.3; Found: 620.3. ^{1}H NMR (500 MHz, DMSO, 343

K) δ 9.3 (bs, 1H), 8.26–8.12 (m, 3H), 7.70 (dd, J = 8.2, 7.0 Hz, 1H), 7.64 (d, J = 7.0 Hz, 1H), 7.50 (td, J = 8.7, 2.6 Hz, 1H), 7.00 (s, 1H), 6.91 (s, 1H), 5.46 (d, J = 2.8 Hz, 1H), 5.07 (s, 1H), 4.78 (s, 2H), 4.01 (s, 1H), 3.45 (s, 1H), 3.32 (bs, 3H), 2.97 (m, 1H), 2.85 (s, 3H), 2.74 (dt, J = 14.2, 7.2 Hz, 1H), 2.67 (d, J = 7.2 Hz, 1H), 2.44–2.36 (m, 2H), 2.32 (d, J = 9.2 Hz, 1H), 2.30 (d, J = 8.9 Hz, 1H), 1.82 (s, 4H), 1.60 (d, J = 9.3 Hz, 1H).

Synthesis of Compound 18. Step 1. tert-Butyl (1R,4R,5S)-5-(7-Bromo-8-(2-cyanoethyl)-6-fluoro-4-(methylthio)-2-((3-oxomorpholino)methyl)-1H-pyrrolo[3,2-c]quinolin-1-yl)-2-azabicyclo[2.1.1]hexane-2-carboxylate) (46). This compound was prepared using Steps 1 and 2 from the synthesis of compound 16 using 4-(prop-2-yn-1-yl)morpholin-3-one as the coupling partner in the Sonongashira coupling. LCMS calculated for $C_{30}H_{34}BrFN_5O_4S$ $(M + H)^+$: m/z = 658.2, 660.2; Found: 658.2, 660.2.

Step 2. tert-Butyl (1R,4R,5S)-5-(8-(2-Cyanoethyl)-6-fluoro-7-(7-fluoronaphthalen-1-yl)-4-(methylthio)-2-((3-oxomorpholino)methyl)-1H-pyrrolo[3,2-c]quinolin-1-yl)-2-azabicyclo[2.1.1]hexane-2-carboxylate (47). To a mixture of 46 (346 mg, 0.525 mmol), 2-(7-fluoronaphthalen-1-yl)-4,4,5,5-tetramethyl-1,3,2-dioxaborolane (172 mg, 0.63 mmol), XPhos Pd G2 (41 mg, 0.053 mmol) and potassium phosphate, tribasic (223 mg, 1.05 mmol) were added dioxane/water (12 mL, 5:1) and the reaction flask was sparged with nitrogen, then stirred at 80 °C for 30 min. The reaction was quenched with water and extracted with ethyl acetate. The organic layer was washed with water and brine, dried over sodium sulfate and concentrated. The crude product was purified by column chromatography (0–100% ethyl acetate in hexanes) to provide the desired product. LCMS calculated for $C_{40}H_{40}F_2N_5O_4S$ $(M + H)^+$: m/z = 724.3; Found: 724.3.

Step 3. 3-(1-((1R,4R,5S)-2-Azabicyclo[2.1.1]hexan-5-yl)-6-fluoro-7-(7-fluoronaphthalen-1-yl)-4-(2-methylpyridin-4-yl)-2-((3-oxomorpholino)methyl)-1H-pyrrolo[3,2-c]quinolin-8-yl)propanenitrile (18). To a solution of 47 (20 mg, 0.028 mmol) in dioxane (0.5 mL) were added Pd(PPh₃)₄ (16 mg, 0.014 mmol), Copper 2-methylsalicylate (21 mg, 0.10 mmol) and 2-methyl-4-(4,4,5,5-tetramethyl-1,3,2-dioxaborolan-2-yl)-pyridine (15 mg, 0.69 mmol) and the reaction was sparged with nitrogen, then stirred at 120 °C for 1 h. The reaction was cooled to r.t. and quenched with sat. at. ammonium hydroxide and extracted with DCM. The organic layer was dried over sodium sulfate and concentrated. The residue was dissolved in 1:1 TFA/DCM (1 mL) and stirred at r.t. for 45 min, then diluted with MeOH and purified by prep-LCMS (XBridge C18 column, eluting with a gradient of acetonitrile/water containing 0.1% TFA, at flow rate of 60 mL/min) to afford the desired product as the corresponding TFA salt (1.2 mg, 6.6%). LCMS calculated for $C_{40}H_{35}F_2N_6O_2$ $(M + H)^+$: m/z = 669.3; Found: 669.3. ¹H NMR (600 MHz, DMSO) δ 9.42 (s, 1H), 8.82 (d, J = 5.6 Hz, 1H), 8.33 (d, J = 12.3 Hz, 1H), 8.26–8.16 (m, 2H), 8.13–7.98 (m, 3H), 7.77–7.66 (m, 2H), 7.55 (dtd, J = 14.4, 8.7, 2.6 Hz, 1H), 7.22–7.03 (m, 1H), 6.89 (dd, J = 10.7, 2.6 Hz, 1H), 5.63–5.50 (m, 1H), 5.14 (dd, J = 15.8, 10.8 Hz, 1H), 4.94 (d, J = 6.0 Hz, 1H), 4.67 (dd, J = 15.9, 9.8 Hz, 1H), 4.21–4.12 (m, 3H), 3.85 (t, J = 5.1 Hz, 2H), 3.47 (s, 1H), 3.31 (dq, J = 13.1, 4.7 Hz, 1H), 3.18 (ddd, J = 12.0, 6.4, 4.2 Hz, 1H), 3.10–3.00 (m, 1H), 2.91 (ddd, J = 12.1, 7.4, 4.3 Hz, 1H), 2.81–2.54 (m, 6H), 2.34 (t, J = 10.1 Hz, 1H), 1.61 (d, J = 9.2 Hz, 1H).

Synthesis of Compound 22. This compound was prepared using the procedures described for compound 23, using 7-fluoronaphthyl boronic acid, pinacol ester in the Suzuki cross

coupling step. LCMS calculated for $C_{40}H_{36}F_2N_7O_2$ $(M + H)^+$: m/z = 684.3; Found: 684.3. ¹H NMR (TFA salt, mixture of atropisomers, rotamers, 600 MHz, DMSO-d_6) δ 9.59 (m, 1H), 9.49 (m, 0.7H), 9.20 (m, 0.3H), 8.82 (m, 1H), 8.40–8.30 (m, 1.5H), 8.27–8.16 (m, 2.5H), 7.87–7.61 (m, 4H), 7.55 (m, 1H), 7.16 (m, 0.5H), 6.92 (m, 0.5H), 5.93 (m, 0.7H), 5.77 (m, 0.3H), 5.67 (m, 0.3H), 5.44 (m, 0.7H), 5.21–4.89 (m, 1H), 4.35–4.12 (m, 2.3H), 4.05–3.38 (m, 3.3H), 3.14–1.86 (m, 11H), 1.74–1.46 (m, 4.4H).

■ ASSOCIATED CONTENT

ⓢ Supporting Information

The Supporting Information is available free of charge at https://pubs.acs.org/doi/10.1021/acs.jmedchem.4c02662.

Detailed synthetic protocols, characterization of final compounds, protocols for *in vitro* and *in vivo* assays, mean and standard deviations for assays, X-ray parameters for compound 3 and 5a (PDF)

Table of molecular formula strings (CSV)

Accession Codes

Accession Codes PDB depositions are available for compound 3 (9E5F) and 5a (9E5D). Authors will release the atomic coordinates and structure factors upon article publication.

■ AUTHOR INFORMATION

Corresponding Author

Alexander Sokolsky — *Department of Discovery Chemistry, Incyte Research Institute, Incyte Corporation, Wilmington, Delaware 19803, United States;* ⓞ orcid.org/0000-0001-9974-8948; Email: asokolsky@incyte.com

Authors

Qinda Ye — *Department of Discovery Chemistry, Incyte Research Institute, Incyte Corporation, Wilmington, Delaware 19803, United States;* Present Address: Superstring Capital Management, New York, New York

Artem Shvartsbart — *Department of Discovery Chemistry, Incyte Research Institute, Incyte Corporation, Wilmington, Delaware 19803, United States*

Zhenwu Li — *Department of Discovery Chemistry, Incyte Research Institute, Incyte Corporation, Wilmington, Delaware 19803, United States;* Present Address: SK Life Sciences, King of Prussia, PA.

Pei Gan — *Department of Discovery Chemistry, Incyte Research Institute, Incyte Corporation, Wilmington, Delaware 19803, United States;* Present Address: Quanta Therapeutics, Radnor, PA.

Rocco L. Policarpo — *Department of Discovery Chemistry, Incyte Research Institute, Incyte Corporation, Wilmington, Delaware 19803, United States*

Chao Qi — *Department of Discovery Chemistry, Incyte Research Institute, Incyte Corporation, Wilmington, Delaware 19803, United States;* Present Address: Synovation Therapeutics, Wilmington, DE.

Jeremy J. Roach — *Department of Discovery Chemistry, Incyte Research Institute, Incyte Corporation, Wilmington, Delaware 19803, United States;* Present Address: SK Life Sciences, King of Prussia, PA.

Wenyu Zhu — *Department of Discovery Chemistry, Incyte Research Institute, Incyte Corporation, Wilmington, Delaware 19803, United States*

Matthew S. McCammant − *Department of Discovery Chemistry, Incyte Research Institute, Incyte Corporation, Wilmington, Delaware 19803, United States*

Bin Hu − *Department of Discovery Chemistry, Incyte Research Institute, Incyte Corporation, Wilmington, Delaware 19803, United States*

Gencheng Li − *Department of Discovery Chemistry, Incyte Research Institute, Incyte Corporation, Wilmington, Delaware 19803, United States*

Haolin Yin − *Department of Discovery Chemistry, Incyte Research Institute, Incyte Corporation, Wilmington, Delaware 19803, United States*

Peter Carlsen − *Department of Discovery Chemistry, Incyte Research Institute, Incyte Corporation, Wilmington, Delaware 19803, United States*

Gia Hoang − *Department of Discovery Chemistry, Incyte Research Institute, Incyte Corporation, Wilmington, Delaware 19803, United States*

Le Zhao − *Department of Discovery Chemistry, Incyte Research Institute, Incyte Corporation, Wilmington, Delaware 19803, United States*

Robert Susick − *Department of Discovery Chemistry, Incyte Research Institute, Incyte Corporation, Wilmington, Delaware 19803, United States*

Fenglei Zhang − *Department of Discovery Chemistry, Incyte Research Institute, Incyte Corporation, Wilmington, Delaware 19803, United States; Present Address: Synovation Therapeutics, Wilmington, DE.*

Cheng-Tsung Lai − *Department of Computational Chemistry, Incyte Research Institute, Incyte Corporation, Wilmington, Delaware 19803, United States*

Abdellah Allali Hassani − *Department of Applied Technology, Incyte Research Institute, Incyte Corporation, Wilmington, Delaware 19803, United States*

Leslie B. Epling − *Department of Applied Technology, Incyte Research Institute, Incyte Corporation, Wilmington, Delaware 19803, United States*

Alexandra Gallion − *Department of Preclinical Pharmacology, Incyte Research Institute, Incyte Corporation, Wilmington, Delaware 19803, United States*

Kerri Kurzeja-Lipinski − *Department of Applied Technology, Incyte Research Institute, Incyte Corporation, Wilmington, Delaware 19803, United States*

Karen Gallagher − *Department of Applied Technology, Incyte Research Institute, Incyte Corporation, Wilmington, Delaware 19803, United States*

Valerie Roman − *Department of Preclinical Pharmacology, Incyte Research Institute, Incyte Corporation, Wilmington, Delaware 19803, United States*

Matthew R. Farren − *Department of Preclinical Pharmacology, Incyte Research Institute, Incyte Corporation, Wilmington, Delaware 19803, United States*

Weixi Kong − *Department of DMB, Incyte Research Institute, Incyte Corporation, Wilmington, Delaware 19803, United States*

Marc C. Deller − *Department of Applied Technology, Incyte Research Institute, Incyte Corporation, Wilmington, Delaware 19803, United States*

Guofeng Zhang − *Department of Applied Technology, Incyte Research Institute, Incyte Corporation, Wilmington, Delaware 19803, United States*

Maryanne Covington − *Department of Applied Technology, Incyte Research Institute, Incyte Corporation, Wilmington, Delaware 19803, United States*

Sharon Diamond − *Department of DMB, Incyte Research Institute, Incyte Corporation, Wilmington, Delaware 19803, United States*

Sunkyu Kim − *Department of Preclinical Pharmacology, Incyte Research Institute, Incyte Corporation, Wilmington, Delaware 19803, United States*

Wenqing Yao − *Department of Discovery Chemistry, Incyte Research Institute and Department of Preclinical Pharmacology, Incyte Research Institute, Incyte Corporation, Wilmington, Delaware 19803, United States; Present Address: Synovation Therapeutics, Wilmington, DE.*

Xiaozhao Wang − *Department of Discovery Chemistry, Incyte Research Institute, Incyte Corporation, Wilmington, Delaware 19803, United States*

Complete contact information is available at:
https://pubs.acs.org/10.1021/acs.jmedchem.4c02662

■ ABBREVIATIONS

ADME, absorption, distribution, metabolism and excretion; AUC, area under the drug concentration−time curve; C_{max}, maximal concentration of the concentration−time curve CYP − cytochrome p450; CYP TDI, time dependent inhibition of cytochrome p450; DIPEA, diisopropyl ethyl amine; DMF, dimethylformamide; ERK, Extracellular signal-regulated kinase; F%, fraction of an administered dose of unchanged drug that reaches systemic circulation; FaSSiF, fasted state simulated intestinal fluid; FDA, Federal Drug Administration; GDP, guanadine diphosphate; GTP, guanadine triphosphate; %HBF, % hepatic blood flow; hERG, human ether-a-go-go-related gene; i.p., intraperitoneal i.v. − intravenous; p.o., per os; MEK, mitogen-activated protein kinase kinase; NIS, N-iodosuccinimide; NMP, N-methylpyrrolidone; SA, structure−activity relationship; SGF, simulated gastric fluid; SOS1, Son of sevenless homologue 1; TEA, triethylamine; THF, tetrahydrofuran; V_{ss}, volume of distribution at steady state

■ REFERENCES

(1) Cox, A. D.; Fesik, S. W.; Kimmelman, A. C.; Luo, J.; Der, C. J. Drugging the undruggable RAS: Mission possible? *Nat. Rev. Drug Discovery* **2014**, *13* (11), 828−851.

(2) Simanshu, D. K.; Nissley, D. V.; McCormick, F. RAS Proteins and Their Regulators in Human Disease. *Cell* **2017**, *170* (1), 17−33.

(3) Prior, I. A.; Lewis, P. D.; Mattos, C. A comprehensive survey of Ras mutations in cancer. *Cancer Res.* **2012**, *72* (10), 2457−2467.

(4) Prior, I. A.; Hood, F. E.; Hartley, J. L. The Frequency of Ras Mutations in Cancer. *Cancer Res.* **2020**, *80* (14), 2969−2974.

(5) Ostrem, J. M.; Peters, U.; Sos, M. L.; Wells, J. A.; Shokat, K. M. K-Ras(G12C) inhibitors allosterically control GTP affinity and effector interactions. *Nature* **2013**, *503* (7477), 548−551.

(6) Fell, J. B.; Fischer, J. P.; Baer, B. R.; Blake, J. F.; Bouhana, K.; Briere, D. M.; Brown, K. D.; Burgess, L. E.; Burns, A. C.; Burkard, M. R.; Chiang, H.; Chicarelli, M. J.; Cook, A. W.; Gaudino, J. J.; Hallin, J.; Hanson, L.; Hartley, D. P.; Hicken, E. J.; Hingorani, G. P.; Hinklin, R. J.; Mejia, M. J.; Olson, P.; Otten, J. N.; Rhodes, S. P.; Rodriguez, M. E.; Savechenkov, P.; Smith, D. J.; Sudhakar, N.; Sullivan, F. X.; Tang, T. P.; Vigers, G. P.; Wollenberg, L.; Christensen, J. G.; Marx, M. A. Identification of the Clinical Development Candidate MRTX849, a Covalent KRAS(G12C) Inhibitor for the Treatment of Cancer. *J. Med. Chem.* **2020**, *63* (13), 6679−6693.

(7) Lanman, B. A.; Allen, J. R.; Allen, J. G.; Amegadzie, A. K.; Ashton, K. S.; Booker, S. K.; Chen, J. J.; Chen, N.; Frohn, M. J.; Goodman, G.; Kopecky, D. J.; Liu, L.; Lopez, P.; Low, J. D.; Ma, V.; Minatti, A. E.; Nguyen, T. T.; Nishimura, N.; Pickrell, A. J.; Reed, A. B.; Shin, Y.; Siegmund, A. C.; Tamayo, N. A.; Tegley, C. M.; Walton, M. C.; Wang, H. L.; Wurz, R. P.; Xue, M.; Yang, K. C.; Achanta, P.; Bartberger, M. D.; Canon, J.; Hollis, L. S.; McCarter, J. D.; Mohr, C.; Rex, K.; Saiki, A. Y.; San Miguel, T.; Volak, L. P.; Wang, K. H.; Whittington, D. A.; Zech, S. G.; Lipford, J. R.; Cee, V. J. Discovery of a Covalent Inhibitor of KRAS(G12C) (AMG 510) for the Treatment of Solid Tumors. *J. Med. Chem.* **2020**, *63* (1), 52−65.

(8) Sacher, A.; LoRusso, P.; Patel, M. R.; Miller, W. H., Jr.; Garralda, E.; Forster, M. D.; Santoro, A.; Falcon, A.; Kim, T. W.; Paz-Ares, L.; et al. Single-Agent Divarasib (GDC-6036) in Solid Tumors with a KRAS G12C Mutation. *N. Engl. J. Med.* **2023**, *389* (8), 710−721.

(9) Ma, X.; Sloman, D. L.; Duggal, R.; Anderson, K. D.; Ballard, J. E.; Bharathan, I.; Brynczka, C.; Gathiaka, S.; Henderson, T. J.; Lyons, T. W.; Miller, R.; Munsell, E. V.; Orth, P.; Otte, R. D.; Palani, A.; Rankic, D. A.; Robinson, M. R.; Sather, A. C.; Solban, N.; Song, X. S.; Wen, X.; Xu, Z.; Yang, Y.; Yang, R.; Day, P. J.; Stoeck, A.; Bennett, D. J.; Han, Y. Discovery of MK-1084: An Orally Bioavailable and Low-Dose KRAS(G12C) Inhibitor. *J. Med. Chem.* **2024**, *67* (13), 11024−11052.

(10) Hollebecque, A.; Kuboki, Y.; Murciano-Goroff, Y. R.; Yaeger, R.; Cassier, P. A.; Heist, R. S.; Fujiwara, Y.; Deming, D. A.; Ammakkanavar, N.; Patnaik, A.; et al. Efficacy and safety of LY3537982, a potent and highly selective KRAS G12C inhibitor in KRAS G12C-mutant GI cancers: Results from a phase 1 study. *J. Clin. Oncol.* **2024**, *42* (3_suppl), 94.

(11) Lorthiois, E.; Gerspacher, M.; Beyer, K. S.; Vaupel, A.; Leblanc, C.; Stringer, R.; Weiss, A.; Wilcken, R.; Guthy, D. A.; Lingel, A.; Bomio-Confaglia, C.; Machauer, R.; Rigollier, P.; Ottl, J.; Arz, D.; Bernet, P.; Desjonqueres, G.; Dussauge, S.; Kazic-Legueux, M.; Lozac'h, M. A.; Mura, C.; Sorge, M.; Todorov, M.; Warin, N.; Zink, F.; Voshol, H.; Zecri, F. J.; Sedrani, R. C.; Ostermann, N.; Brachmann, S. M.; Cotesta, S. JDQ443, a Structurally Novel, Pyrazole-Based, Covalent Inhibitor of KRAS(G12C) for the Treatment of Solid Tumors. *J. Med. Chem.* **2022**, *65* (24), 16173−16203.

(12) Ban, H. S.; Usui, T.; Nabeyama, W.; Morita, H.; Fukuzawa, K.; Nakamura, H. Discovery of boron-conjugated 4-anilinoquinazoline as a prolonged inhibitor of EGFR tyrosine kinase. *Org. Biomol. Chem.* **2009**, *7* (21), 4415−4427.

(13) Tsukiji, S.; Hamachi, I. Ligand-directed tosyl chemistry for in situ native protein labeling and engineering in living systems: From basic properties to applications. *Curr. Opin. Chem. Biol.* **2014**, *21*, 136−143.

(14) Jiang, L.; Menard, M.; Weller, C.; Wang, Z.; Burnett, L.; Aronchik, I.; Steele, S.; Flagella, M.; Zhao, R.; Evans, J. W. W.; Chin, S.; Chou, K.-J.; Mu, Y.; Longhi, M.; McDowell, L.; Knox, J. E.; Gill, A.; Smith, J. A.; Singh, M.; Quintana, E.; Jiang, J. Abstract 526: RMC-9805, a first-in-class, mutant-selective, covalent and oral KRASG12D(ON) inhibitor that induces apoptosis and drives tumor regression in preclinical models of KRASG12D cancers. *Cancer Res.* **2023**, *83*, 526−526.

(15) Wang, X.; Allen, S.; Blake, J. F.; Bowcut, V.; Briere, D. M.; Calinisan, A.; Dahlke, J. R.; Fell, J. B.; Fischer, J. P.; Gunn, R. J.; Hallin, J.; Laguer, J.; Lawson, J. D.; Medwid, J.; Newhouse, B.; Nguyen, P.; O'Leary, J. M.; Olson, P.; Pajk, S.; Rahbaek, L.; Rodriguez, M.; Smith, C. R.; Tang, T. P.; Thomas, N. C.; Vanderpool, D.; Vigers, G. P.; Christensen, J. G.; Marx, M. A. Identification of MRTX1133, a Noncovalent, Potent, and Selective KRAS(G12D) Inhibitor. *J. Med. Chem.* **2022**, *65* (4), 3123−3133.

(16) Hallin, J.; Bowcut, V.; Calinisan, A.; Briere, D. M.; Hargis, L.; Engstrom, L. D.; Laguer, J.; Medwid, J.; Vanderpool, D.; Lifset, E.; Trinh, D.; Hoffman, N.; Wang, X.; David Lawson, J.; Gunn, R. J.; Smith, C. R.; Thomas, N. C.; Martinson, M.; Bergstrom, A.; Sullivan, F.; Bouhana, K.; Winski, S.; He, L.; Fernandez-Banet, J.; Pavlicek, A.; Haling, J. R.; Rahbaek, L.; Marx, M. A.; Olson, P.; Christensen, J. G. Anti-tumor efficacy of a potent and selective non-covalent KRAS-(G12D) inhibitor. *Nat. Med.* **2022**, *28* (10), 2171−2182.

(17) Cheng, H.; Li, P.; Chen, P.; Irimia, A.; Bae, J. H.; Brooun, A.; Fagan, P.; Lam, R.; Lin, B.; Zhang, J.; et al. Structure-Based Design and Synthesis of Potent and Selective KRAS G12D Inhibitors. *ACS Med. Chem. Lett.* **2023**, *14*, 1351−1357.

(18) Kim, D.; Herdeis, L.; Rudolph, D.; Zhao, Y.; Bottcher, J.; Vides, A.; Ayala-Santos, C. I.; Pourfarjam, Y.; Cuevas-Navarro, A.; Xue, J. Y.; Mantoulidis, A.; Broker, J.; Wunberg, T.; Schaaf, O.; Popow, J.; Wolkerstorfer, B.; Kropatsch, K. G.; Qu, R.; de Stanchina, E.; Sang, B.; Li, C.; McConnell, D. B.; Kraut, N.; Lito, P. Pan-KRAS inhibitor disables oncogenic signalling and tumour growth. *Nature* **2023**, *619* (7968), 160−166.

(19) Tanada, M.; Tamiya, M.; Matsuo, A.; Chiyoda, A.; Takano, K.; Ito, T.; Irie, M.; Kotake, T.; Takeyama, R.; Kawada, H.; Hayashi, R.; Ishikawa, S.; Nomura, K.; Furuichi, N.; Morita, Y.; Kage, M.; Hashimoto, S.; Nii, K.; Sase, H.; Ohara, K.; Ohta, A.; Kuramoto, S.; Nishimura, Y.; Iikura, H.; Shiraishi, T. Development of Orally Bioavailable Peptides Targeting an Intracellular Protein: From a Hit to a Clinical KRAS Inhibitor. *J. Am. Chem. Soc.* **2023**, *145* (30), 16610−16620.

(20) Jiang, J.; Jiang, L.; Maldonato, B. J.; Wang, Y.; Holderfield, M.; Aronchik, I.; Winters, I. P.; Salman, Z.; Blaj, C.; Menard, M.; Brodbeck, J.; Chen, Z.; Wei, X.; Rosen, M. J.; Gindin, Y.; Lee, B. J.; Evans, J. W.; Chang, S.; Wang, Z.; Seamon, K. J.; Parsons, D.; Cregg, J.; Marquez, A.; Tomlinson, A. C. A.; Yano, J. K.; Knox, J. E.; Quintana, E.; Aguirre, A. J.; Arbour, K. C.; Reed, A.; Gustafson, W. C.; Gill, A. L.; Koltun, E. S.; Wildes, D.; Smith, J. A. M.; Wang, Z.; Singh, M. Translational and Therapeutic Evaluation of RAS-GTP Inhibition by RMC-6236 in RAS-Driven Cancers. *Cancer Discovery* **2024**, *14* (6), 994−1017.

(21) Niida, A.; Sasaki, S.; Yonemori, K.; Sameshima, T.; Yaguchi, M.; Asami, T.; Sakamoto, K.; Kamaura, M. Investigation of the structural requirements of K-Ras(G12D) selective inhibitory peptide KRpep-2d using alanine scans and cysteine bridging. *Bioorg. Med. Chem. Lett.* **2017**, *27* (12), 2757−2761.

(22) Sogabe, S.; Kamada, Y.; Miwa, M.; Niida, A.; Sameshima, T.; Kamaura, M.; Yonemori, K.; Sasaki, S.; Sakamoto, J. I.; Sakamoto, K. Crystal Structure of a Human K-Ras G12D Mutant in Complex with GDP and the Cyclic Inhibitory Peptide KRpep-2d. *ACS Med. Chem. Lett.* **2017**, *8* (7), 732−736.

(23) Li, L.; Feng, J.; Ren, P.; Liu, Y. *Substituted Quinazoline Compounds and Methods of Use.* WO 2,017,172,979 A1, 2017.

(24) Wang, X.; Zhu, W.; Yang, J.; He, C.; Zhang, F.; Han, H.; Zhao, L.; Li, Y.; Gan, P.; Qi, C., et al. *Tricyclic Compounds as Inhibitors of KRAS.* WO 2,021,142,252 A1, 2021.

(25) Fell, J. B.; Fischer, J. P.; Baer, B. R.; Ballard, J.; Blake, J. F.; Bouhana, K.; Brandhuber, B. J.; Briere, D. M.; Burgess, L. E.; Burkard, M. R.; Chiang, H.; Chicarelli, M. J.; Davidson, K.; Gaudino, J. J.; Hallin, J.; Hanson, L.; Hee, K.; Hicken, E. J.; Hinklin, R. J.; Marx, M. A.; Mejia, M. J.; Olson, P.; Savechenkov, P.; Sudhakar, N.; Tang, T. P.; Vigers, G. P.; Zecca, H.; Christensen, J. G. Discovery of Tetrahydropyridopyrimidines as Irreversible Covalent Inhibitors of KRAS-G12C with In Vivo Activity. *ACS Med. Chem. Lett.* **2018**, *9* (12), 1230−1234.

(26) Veber, D. F.; Johnson, S. R.; Cheng, H. Y.; Smith, B. R.; Ward, K. W.; Kopple, K. D. Molecular properties that influence the oral

bioavailability of drug candidates. *J. Med. Chem.* **2002**, *45* (12), 2615−2623.

(27) Grela, K.; Michalska, M. Simple and Mild Synthesis of Indoles via Hydroamination Reaction Catalysed by NHC−Gold Complexes: Looking for Optimized Conditions. *Synlett* **2016**, *27* (4), 599−603.

(28) Liebeskind, L. S.; Srogl, J. Heteroaromatic thioether-boronic acid cross-coupling under neutral reaction conditions. *Org. Lett.* **2002**, *4* (6), 979−981.

(29) Egi, M.; Liebeskind, L. S. Heteroaromatic thioether-organo-stannane cross-coupling. *Org. Lett.* **2003**, *5* (6), 801−802.